

Politecnico di Milano
Final Report
Space Systems Engineering and Operations
Prof. Roberta Michèle Lavagna
(A.Y. 2022/23)

Group: 39

Pietro Bosco (10643020)
Tommaso Brombara (10682041)
Riccardo Cadamuro (10702567)
Álvaro Flórez González (10911708)
Emanuele Marzorati (10724126)
Daniele Peruzzotti (10702005)

June 2023



POLITECNICO
MILANO 1863

Contents

1. Assignment 1: System overview and MA subsystem	1
1.1 Introduction	1
1.2 Mission goals and drivers	1
1.3 Functional analysis	1
1.3.1 Functional Decomposition	1
1.3.2 Requirements	2
1.4 Phases and Concept of Operations	3
1.4.1 Launch and escape from Earth gravitational field	4
1.4.2 Reach and insert in the orbit around Mercury	4
1.4.3 Orbit around Mercury	5
1.4.4 Disposal	6
1.5 On board instruments	6
1.5.1 Payload	6
1.5.2 Flybys and orbital operations	7
1.6 Mission Analysis	8
1.6.1 Launch and Earth escape	8
1.6.2 Interplanetary leg	8
1.6.3 Mercury orbit	8
1.6.4 ΔV estimations	9
1.6.5 Δt estimations	9
2. Assignment 2: Propulsion subsystem	10
2.1 Architecture	10
2.1.1 Tanks	10
2.1.2 Propellant supply	10
2.1.3 Thrusters	11
2.2 Primary and Secondary Propulsion	11
2.3 Justification of the selected propulsion type	12
2.3.1 Operations / Phases	12
2.3.2 DeltaV budget breakdown	13
2.4 Reverse Sizing	14
2.4.1 Propellant selection and masses	14
2.4.2 Tanks sizing	15
2.4.3 Pressurant selection and masses	16
2.4.4 Feeding subsystem sizing	16
3. Assignment 3: TTMTTC subsystem	17
3.1 TTMTTC Architecture	17
3.2 Mission phases and operations	18
3.3 Reverse Sizing	20
3.3.1 Losses	20
3.3.2 Antennas	20
3.3.3 Link budget	21
4. Assignment 4: AOCS subsystem	23
4.1 Architecture	23
4.1.1 Sensors	23
4.1.2 Actuators	24
4.2 Pointing Budget for Control	25
4.2.1 Control Modes	25
4.2.2 Pointing budget	26
4.3 Disturbances	26
4.3.1 External Disturbances	26
4.3.2 Internal Disturbances	26
4.4 Reverse Sizing	27
4.4.1 Subsystem mass sizing	27
4.4.2 Reaction wheels sizing	27

4.4.3 Thruster sizing	28
4.4.4 Mass budget	29
5. Assignment 5: TCS subsystem	30
5.1 Introduction	30
5.2 Architecture	30
5.2.1 Sunshade	30
5.2.2 Multilayered insulation	30
5.2.3 Radiators	30
5.2.4 Heaters	31
5.2.5 Structure	31
5.3 Phases	31
5.3.1 Cruise phase	31
5.3.2 Orbital phase	32
5.4 Reverse Sizing	32
5.4.1 Thermal environment	32
5.4.2 Spacecraft modeling	33
5.4.3 Allowable temperature range	34
5.4.4 Critical cases	34
5.4.5 Mass estimation	35
5.4.6 Material choice	36
6. Assignment 6: EPS subsystem	37
6.1 EPS components	37
6.1.1 Solar Array	37
6.1.2 Battery	38
6.1.3 Power System Electronics	38
6.1.4 Solar Array Junction Box	38
6.1.5 Power Distribution Unit	38
6.1.6 Solar Array Drive Assembly	39
6.2 Architecture	39
6.2.1 Electrical power per phase	39
6.2.2 Eclipse management	40
6.2.3 Power regulation	40
6.3 Reverse Sizing	40
6.3.1 Primary source selection and sizing	40
6.3.2 Secondary source selection and sizing	42
7. Assignment 7: CONF and OBDH subsystem	44
7.1 Configuration	44
7.1.1 Space Segment	44
7.2 On-Board Data Handling	47
7.2.1 Architecture	47
7.2.2 Reverse Sizing	49

Change log	
§1.3.2	pp. 2-3: made explicit that requirements have been derived by the team, -not copied- from literature and the link between them and the functionalities
§1.4	pp. 3-6: added Gantt chart for ConOps, added link between phases and functionalities
§1.4.2	pp. 4-5: update ConOps, added spacecraft deployment and activation, science during flybys, DSM duration
§1.5.2	pp. 7: added details about payload ConOps in Mercury orbit
§1.6.4	pp.9: added details on the ΔV reverse sizing and Keplerian elements used
§3	pp. 17-21: added more references to the bibliography
§3.1	pp. 17: more details about the frequency selection
§3.2	pp. 19: Fig.3.1 explained more in detail
§3.3.1, §3.3.2	pp. 20-21: added dimensions used in the computations, added explanation about the Phased Array Antenna gain estimation.
§3.3.3	pp. 21-22: better justification for the link budget margin, for the zero peaks the procedure in the computation of the link budget in Fig.3.2a and Fig.3.2b, added analysis on the bandwidth
§3.3.4	removed
§4.1.1	pp. 24: more detailed analysis of the sensors suites and IMU selection
§4.1.2	pp. 25: more detailed analysis of the thrusters set
§4.2.1	pp. 25: more details about sensors utilization in Operational (OP) and Safe Hold (SH) modes
§5	pp. 32-33: added in-text references to the bibliography
§5.4.1, §5.4.2	pp. 32-33: better explanation of data used in reverse sizing, added Eq. 5.8, added spacecraft dimensions in Tab. 5.1
§5.4.3	pp. 34: better explanation of the temperature margins used in the computations
§5.4.4	pp. 35: more details about the Heaters heat flux reverse sizing
§6.3.1	pp. 41-42: added results of the intermediate parameters, added explanation to the power margin, table 6.4 revised, added clarification about OSR area with respect to the solar cells
§6.3.2	pp. 42-43: added results of the intermediate parameters

Assignment 1: System overview and MA subsystem

1.1 Introduction

MESSENGER (Mercury Surface, Space Environment, Geochemistry and Ranging) belongs to the NASA *Discovery* program, founded in 1990 that aims to investigate specific scientific questions about the Solar system but with lower costs with respect to previous programs like *New Frontiers*. Even though Mercury had already been reached by Mariner 10 in 1973, in that occasion the spacecraft was only able to perform three flybys of Mercury and to map the 40 – 45 % of its surface, while Messenger aimed to orbit around Mercury for one Earth year, which was later extended to just over four years.

The mission was launched on 3 August 2004 on a Delta II 7925 launch vehicle from Cape Canaveral and reached the heliocentric orbit 57 minutes later.

Messenger reached Mercury on 18 March 2011, after almost seven years of interplanetary travel that involved one flyby of the Earth, two flybys of Venus, three flybys of Mercury itself and five Deep Space Manoeuvres.

1.2 Mission goals and drivers

MESSENGER mission is designed to answer six fundamental questions regarding Mercury: (1) What planetary formation processes led to Mercury's high ratio of metal to silicate? (2) What is the geological history of Mercury? (3) What are the nature and origin of Mercury's magnetic field? (4) What are the structure and state of Mercury's core? (5) What are the radar-reflective materials at Mercury's poles? (6) What are the important volatile species and their sources and sinks near Mercury?

These guiding questions can be translated into six objectives[9][2]:

1. Map the elemental and mineralogical composition of Mercury's surface;
2. Image globally the surface at a resolution of hundreds of meters or better;
3. Determine the structure of the planet's magnetic field;
4. Measure the libration amplitude and gravitational field structure;
5. Determine the composition of the radar-reflective materials at Mercury's poles;
6. Characterize exosphere neutrals and accelerated magnetosphere ions;

Due to the high complexity of the mission, both in terms of ΔV required to follow the interplanetary trajectory and for station-keeping (2300 m/s)[7][10] and in terms of survival in the harsh thermal environment around Mercury during the orbital phase of the mission, those two aspects have been pointed out as mission drivers.

1.3 Functional analysis

The mission requires four main functionalities which cover its complete time-span and operations. In particular the first one consists in *reaching and keeping the orbit around Mercury* that regards each aspect about the interplanetary travel and the orbiting around Mercury from the flight dynamics point of view. Moreover, in order to succeed in the high level goals, two more functionalities are needed: *collecting scientific data*, which is actually the mission main objective, and *transmitting them to the Earth*. Eventually, an *end of mission* functionality is prescribed according to the planetary protection principles, in particular, Mercury belongs to the first *COSPAR* category allowing for the disposal of the spacecraft by crushing it on the planet surface.

1.3.1 Functional Decomposition

This section contains a detailed functional decomposition of the mission.

1. Reach and keep orbit around Mercury
 - 1.1 Accelerate the SC out of Earth's gravity well;
 - 1.2 Guide the SC to Mercury along the interplanetary leg;
 - 1.3 Survive the interplanetary environment;

- 1.4 Perform the capture maneuver on Mercury;
- 1.5 Maintain the prescribed orbit around Mercury for the time necessary to complete the scientific mission;
- 1.6 Withstand Mercury's orbit harsh environmental conditions during the whole mission;
2. Collect scientific data
 - 2.1 Activate and calibrate all the scientific instruments, map the elemental and mineralogical composition of Mercury's surface;
 - 2.2 Image globally the surface at resolution of hundreds of meters or better;
 - 2.3 Determine the structures of the planet's magnetic field;
 - 2.4 Measure the libration amplitude and gravitational field structure;
 - 2.5 Determine the composition of the radar reflective materials at Mercury's poles;
 - 2.6 Characterize exosphere neutrals and accelerated magnetosphere ions;
3. Transmit data to Earth
 - 3.1 Store collected data onboard until transmission window open;
 - 3.2 Transmit correctly data to Earth;
 - 3.3 Validate the data received;
4. End of the mission
 - 4.1 Stop performing propulsive orbital corrections;
 - 4.2 Complete all data transmissions;
 - 4.3 Crash into the Mercury's surface;

1.3.2 Requirements

The following section contains the high level requirements that have been derived by the team from the available literature by analyzing what functions needed to be performed to achieve the planned mission goals and therefore a plausible mission requirement for different subsystems. These were then divided by the previously cited functionalities [10][7]:

Reach and keep orbit around Mercury

ID	Requirement	Function(s)
R-OP-010	SC hardware components shall be picked among space-hardened ones;	1
NH-OP-011	SC hardware components should be picked among flight proven ones (TRL 9) to reduce mission cost;	
R-MA-010	Launcher choice shall provide an energy $c_3=16.4 \text{ km}^2/\text{s}^2$ to the SC;	1.1
R-MA-020	GNC and Propulsion systems shall allow the SC to follow the planned interplanetary trajectory;	1.2, 1.3
R-PS-010	Propulsion system shall provide at least 2300 m/s [7][10] of Δv ;	
R-PS-020	Propulsion system shall be capable of performing precise impulses of more than 10m/s after years of inactivity;	
R-PS-030	Propulsion system shall be capable of periodically correcting SC orbit and attitude to account for perturbances;	1.2, 1.4, 1.5
R-EPS-010	Electric system shall be capable of maintaining SC in hibernation state for up to 7 years in deep space;	
R-EPS-020	SC shall have enough battery power to survive 35min eclipse;	1.3, 1.5, 1.6
R-OBDH-010	Electronic system (IEM, Integrated Electronics Module) should be built with redundancy;	
R-TCS-010	Thermal protection system shall protect SC components from intense heat at 0.3AU from the Sun and in proximity of Mercury's surface.	

Collect scientific data

ID	Requirement	Function(s)
R-ADCS-010	ADCS system shall be capable of orienting the spacecraft correctly to accommodate both ASP and NTSP;	2
R-EPS-030	Solar panels shall provide at least 640W of power at EOL around Mercury [7];	
R-MA-030	SC orbit shall be picked in such a way to transit through the whole magnetosphere;	2.3, 2.6
R-MA-040	SC shall be placed in an orbit that allows for an analysis of Mercury's polar regions;	2.5
R-PLD-010	Total instruments mass shall not exceed 50kg;	2
R-PLD-020	Onboard instruments shall be able to produce a global map of the surface Mercury with a resolution of at least 2.4 km/pixel in color and 500 m/pixel in B and W;	2.2
R-PLD-030	Onboard magnetometer shall be placed at least 3.5m from the main SC body;	2.3
R-PLD-040	Onboard instruments shall be able to perform altimetric measurements of the planet;	2.4, 2.5
R-PLD-050	Onboard instruments shall be able to perform UV, gamma-ray and neutron spectrometry of the polar regions;	2.1, 2.5
R-PLD-060	Onboard instruments should be picked such that measures can be crosschecked with the data from other onboard instruments.	2.1

Transmit data to Earth

ID	Requirement	Function(s)
R-OBDH-020	SC shall have at least 8GB internal memory storage to store scientific data until transmission;	3.1
R-OBDH-030	SC shall be able to perform data collection autonomously;	3
R-TTMTC-010	Communications system shall be capable of communicating both near Earth (hundreds of Km) and at 1.4AU;	
R-TTMTC-020	SC shall be able to transmit and receive telemetry data and commands;	3.2
R-TTMTC-030	Telemetry downlink shall have adjustable bit rate depending on mission phase and SC state;	
R-TTMTC-040	Transmission system shall be able to encrypt and decrypt data;	3.2, 3.3
R-TTMTC-050	Transmission system shall be able to communicate with Earth through DSN.	3

End of the mission

ID	Requirement	Function(s)
R-MA-050	SC shall be placed in an orbit that will cause it to fall on Mercury to safely dispose of itself;	4
R-FUN-010	SC shall be designed in such a way not to leave any debris in Mercury's orbit.	

1.4 Phases and Concept of Operations

The mission profile has been divided by the team into four main phases based on a literature survey [1][6][5], for each of them the Concept of Operations (ConOps) has been derived.

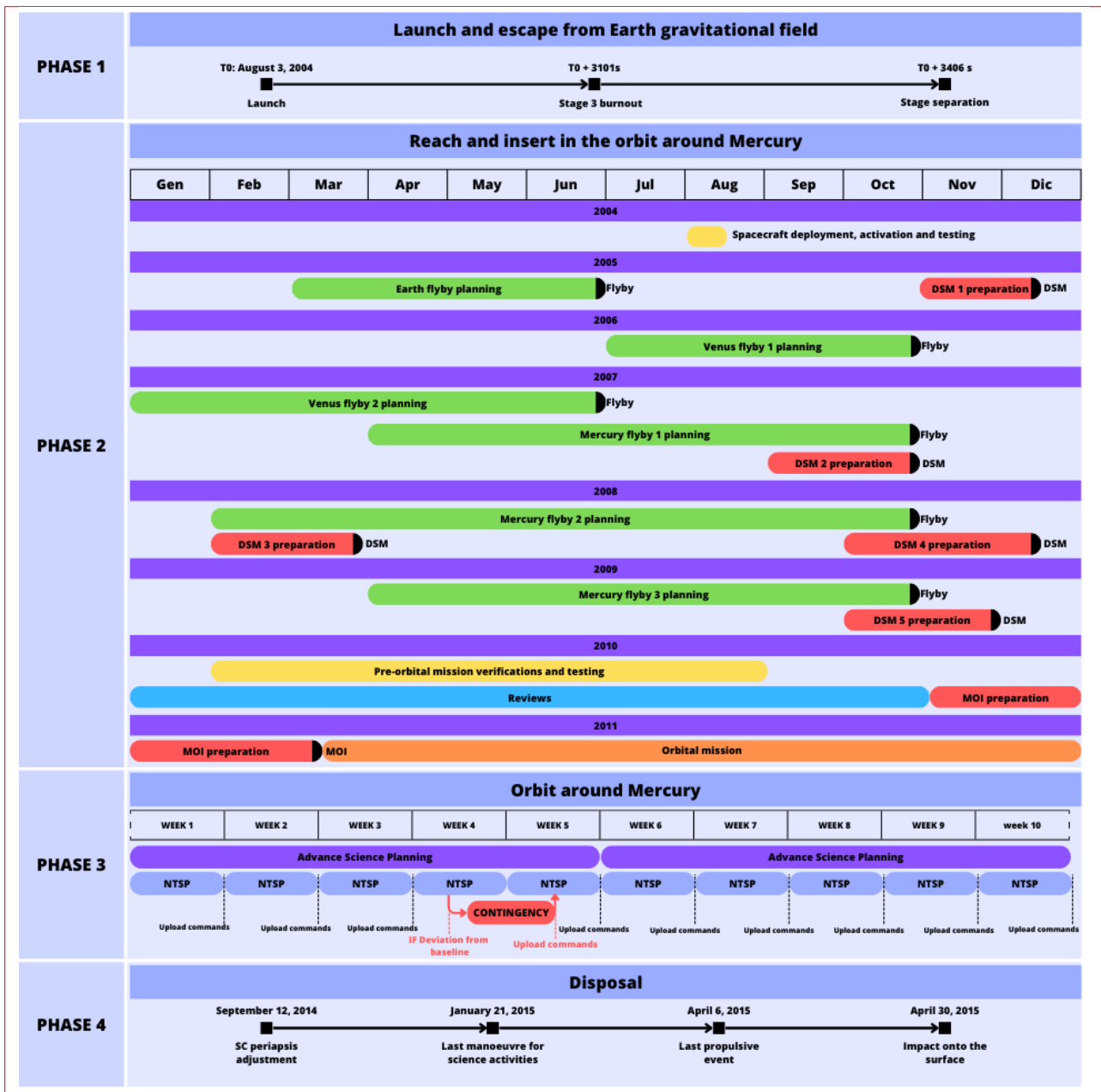


Figure 1.1: Messenger ConOps Gantt chart

1.4.1 Launch and escape from Earth gravitational field

- Launch, $T + 0s$, *August 3, 2004*: the launch will occur from Cape Canaveral, Florida on a Delta II 7925 launcher;
- Stage 3 burnout, $T + 3101s$: the last stage of the launcher finishes its propellant after having placed the spacecraft in the heliocentric trajectory;
- Stage 3 separation, $T + 3406s$: the spacecraft detaches from the launcher and is ready to begin its mission.

The operations described in this phase fulfill the functionalities 1.1, 1.2 and 3 (it is always necessary to maintain communication between the SC and the GS).

1.4.2 Reach and insert in the orbit around Mercury

- Spacecraft deployment and activation, *August 3/6, 2004*: Spacecraft is brought under full 3 axis control, solar panels are deployed and onboard systems are powered up one by one on orbit for the first time. Contact with the ground station is established through omnidirectional antennas;

- Testing of onboard systems, *August 3/9, 2004*: the SC will perform tests on the onboard systems and instrumentation for the first 6 days of flight before being considered fully operative;
- Earth flyby, *August 02, 2005*: decreases the heliocentric orbit periapsis to follow its interplanetary path;
 - Science during Earth flyby: perform instruments calibration, Earth and Moon imaging and observations, magnetic field measurements and testing of the RF subsystem.
- DSM 1, *December 12, 2005*, *Duration: 522 s*: corrects the heliocentric trajectory to perform correctly the first rendez-vous with Venus;
- Venus flyby 1, *October 24, 2006*: increases SC orbit inclination and reduces its period to almost exactly the Venus orbit period;
- Venus flyby 2, *June 5, 2007*: lowers the orbit periapsis enough to enable Mercury flyby;
 - Science during Venus flybys: instrument testing, measure the atmospheric species and their chemical properties, the interplanetary magnetic field and perform observation on the charged particles at the Venus bowshock.
- DSM 2, *October 17, 2007*, *Duration: 518 s*: corrects the trajectory and encounter Mercury for the first flyby;
- Mercury flyby 1, *January 14, 2008*: reduces the SC arrival velocity to Mercury;
- DSM 3, *March 17, 2008*, *Duration: 150 s*: major trajectory correction after the flyby;
- Mercury flyby 2, *October 6, 2008*: reduces the SC arrival velocity to Mercury;
- DSM 4, December 4/8, 2008, *Duration: 385 s*: major trajectory correction after the flyby;
- Mercury flyby 3, *September 29, 2009*: reduces the SC arrival velocity to Mercury;
 - Science during Mercury flybys: partial mapping of the surface of Mercury, measurements of the magnetic field and of the chemical species in the exosphere and in the magnetotail.
- DSM 5, *November 24, 2009*, *Duration: 245 s*: major trajectory correction after the flyby;
- Mercury Capture, *March 18, 2011*, *Duration: 885 s*: capture manoeuvre and insertion in the orbit around Mercury enabling the primary science mission to begin.

The operations related to the payload activities and scientific observations performed during flybys and during the orbital phase around Mercury are more in depth analyzed in section 1.5.2.

During the interplanetary cruise, the concept of operations prescribes a moderate DSN tracking in quiet cruise periods and additional tracking near critical events such as gravity assist flyby and deep space maneuvers. Communications are established well in advance of each critical activities such as deep space maneuvers or fly-bys. Orbit determination in this phase relies primarily on the DSN, on approach to Venus and Mercury, this data will be augmented with DeltaDOR and optical navigation measurements. The DSN long range planning includes periods for obtaining measurements each week starting five weeks prior to each flyby. After each Orbit Determination solution, the navigation team will perform a mapping of the trajectory and its uncertainties.

After each propulsive maneuver, the remaining trajectory is re-optimized to obtain the most fuel efficient and lowest risk solution possible. The operations described in this phase fulfill the functionalities 1.2, 1.3, 1.4, 2.1 and 3.

1.4.3 Orbit around Mercury

In this phase, all the activities are scheduled and performed in two modes: the Advanced Science Planning (ASP) regarding long term period operation, this assessment will be performed every 5 weeks, each time producing an updated baseline for the remainder of the mission; and a short-term scheduling process known as Near Term Science Planning (NTSP).

ASP: the output of ASP process is the long-range plan of all instruments and associated spacecraft GNC activities that span entirely the nominal one-year orbital mission, in this process it is defined the set of measurement requirements to fulfill the mission science goals considering that very often the pointing and orientation of one instrument will conflict with those of another. The ASP will in general deal with the required Orbital Correction Maneuver to be performed every 88 Earth days to recover the orbital path from the solar radiation perturbation.

NTSP: it contains the short term optimized scheduling for the orbital ConOps. In this mode, command sequences are sent to operate the spacecraft subsystems considering weekly updates. The preparation of

each one-week command sequence requires three weeks of planning. Each request of change in the spacecraft pointing is referred to the ASP process.

CONTINGENCY PLANNING: due to the harsh environment in the vicinity of Mercury and the mission profile that heavily constrains the spacecraft control, power generation, data downlink and observation opportunities, deviations from the baseline may result in very problematic situations. Contingency plans, once devised, can be directly inserted into the next ASP cycle or, for more pressing cases, being immediately inserted into the upcoming NTSP cycle.

The operations described in this phase fulfill the functionalities 1.5, 1.6, 2, 3.

1.4.4 Disposal

- SC orbit periapsis adjustment *September 12, 2014*: the periapsis altitude is set to 25 km;
- Orbit rising *January 21, 2015*: last maneuver to raise SC orbit for science activities;
- Last propulsive event, *April 6, 2015*: SC runs completely out of propellant, pressurizing Helium is used for propulsion, SC speed is increased by 8.9 m/s;
- Disposal, *April 30, 2015*: impact onto the surface of Mercury with velocity 3.911 km/s.

The operations described in this phase fulfill the functionalities 4.

1.5 On board instruments

1.5.1 Payload

MESSENGER carries seven scientific instruments and a radio science experiment in order to return the data collected from Mercury orbit[13] [14].

	Mass	Power	Development
MDIS	8.0 kg	7.6 W	The Johns Hopkins University Applied Physics Laboratory
GRS	9.2 kg	16.5 W	The Johns Hopkins University Applied Physics Laboratory, Patriot Engineering, Lawrence Berkeley National Laboratory, Lawrence Livermore National Laboratory
NS	3.9 kg	6.0 W	The Johns Hopkins University Applied Physics Laboratory, Patriot Engineering, Los Alamos National Library
XRS	3.4 kg	6.9 W	The Johns Hopkins University Applied Physics Laboratory
MAG	4.4 kg	4.2 W	NASA Goddard Space Flight Center and the Johns Hopkins University Applied Laboratory
MLA	7.4 kg	16.4 W	NASA Goddard Space Flight Center
MASCS	3.1 kg	6.7 W	Laboratory for Atmospheric and Space Physics, University of Colorado, Boulder
EPPS	3.1 kg	7.8 W	The Johns Hopkins University Applied Physics Laboratory and University of Michigan, Ann Arbor

Table 1.1: *Payload specifics*

- **MDIS:** Mercury Dual Imaging System, with a wide- and a narrow- angle cameras, will map the landforms and spectral variations on the planet's surface in monochrome, color, and stereo. Multi-spectral imaging will help scientists investigate the different rock types which form Mercury's surface;
- **GRNS:** the Gamma-Ray Spectrometer (**GRS**) measures gamma rays emitted by the nuclei of atoms on the surface that are struck by cosmic rays, while the Neutron Spectrometer (**NS**) maps the variations in the fast, thermal and epithermal neutrons emitted by the surface. The device will look for hydrogen and other geologically important elements;
- **XRS:** the X-Ray Spectrometer will map the elements in the top millimeter of Mercury's crust detecting the x-ray emissions coming from the surface when solar x-rays hit the planet;

- **MAG**: a Magnetometer which will help the scientists to characterize Mercury's magnetic field in detail;
- **MASC**: the Mercury Atmospheric and Surface Composition Spectrometer combines an ultraviolet spectrometer and infrared spectrograph, measuring the abundance of atmospheric gases around Mercury, determining the composition and structure of the planet's thin exosphere, and detect minerals in its surface materials;
- **MLA**: the Mercury Laser Altimeter uses an infrared laser transmitter and a receiver in order to map Mercury's landforms. Moreover, the data will also be used to track the planet's libration - a wobble around its spin axis - which will tell the researchers about the state of Mercury's core;
- **EPPS**: the Energetic Particle and Plasma Spectrometer is meant to measure the mix and features of charged particles in and around Mercury's magnetosphere;
- **Radio Science Experiment**: the Radio Science observations will precisely measure MESSENGER's speed and distance from Earth. This will help the researchers to compute Mercury's gravity field and to support the laser altimeter investigation to determine size and condition of the planet's core. The investigation through the Radio Science experiment is conducted by NASA's Goddard Space Flight Center.

1.5.2 Flybys and orbital operations

The onboard instruments will allow MESSENGER to reach its mission's high level goals, returning the researchers data about Mercury. However, the whole payload apparatus is meant to operate throughout the entire mission flow[3].

Earth flyby

The event provided important calibration opportunities for four MESSENGER instruments. **MDIS** will take images of both the Moon and the Earth; **MASC** will perform spectral observations of the Moon and of the Earth's hydrogen corona; **MAG** will measure the magnetic field and charged particles characteristics; **MLA** will test the efficiency of the transmitter and the receiver, even though it will have already started working before the flyby event.

Venus flyby

Elements of MESSENGER's equipment will be tested during the second Venus flyby. **MDIS** will image both the approaching and departing emispheres; **MASC**'s ultra-violet and infra-red spectrometers will make profiles of the atmospheric species and sense their chemical properties; **MLA** will serve as a passive radiometer; **EPPS** will observe charged particles acceleration at the Venus bowshock and elsewhere; **MAG** will provide measurements of the upstream interplanetary magnetic field.

Mercury flybys and orbit

Science observations will take place during the three Mercury flybys and in the orbit, involving all the components of the MESSENGER's payload; previously unseen regions of the planet will be mapped during the flybys, while the remaining data will be obtained over the four Mercury years (one Earth year) to be spent on orbit. The spacecraft orbital period is 12 hours; science data will be collected for 16 hours of each 24 hours period (two orbits) and then downlinked during a tracking pass which is planned for a time window of 8 hours. The selection of the payloads is driven by the functionalities that depend on the main goals of the mission. In Table 4.1 the main relations between the instruments and the functionalities are presented.

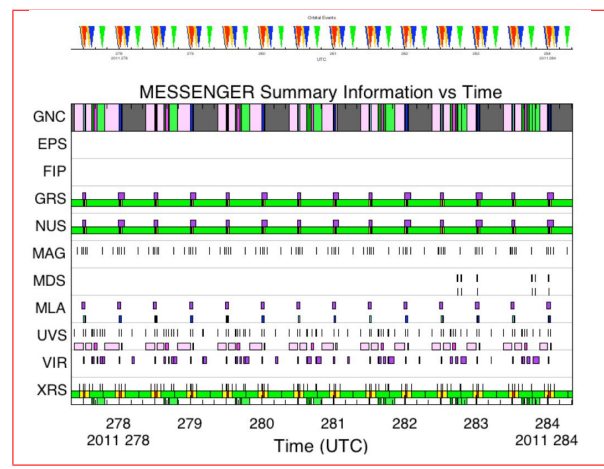


Figure 1.2: Example of Payload ConOps during the orbital phase

Figure 1.2 shows the Concept of Operations for the different instruments onboard the spacecraft during an average week in Mercury orbit. Not all instruments can be used simultaneously due to their relative positions and their different targeting needs, but overlap between different instruments measurements can occur. Different colors refer to different functions performed by the same instrument [1].

Map the elemental and mineralogical composition of Mercury's surface	MDIS, XRS, GRNS, MASCS
Image globally the surface at a resolution of hundreds of meters or better	MDIS
Determine the structure of the planet's magnetic field	MAG, EPPS
Measure the libration amplitude and gravitational field structure	MLA, RS
Determine the composition of the radar-reflective materials at Mercury's poles	GRNS, EPPS
Characterize exosphere neutrals and accelerated magnetosphere ions	MASCS, EPPS

Table 1.2: *MESSENGER science goals and related instruments*

1.6 Mission Analysis

1.6.1 Launch and Earth escape

Given the necessity of C3 energy for the mission, the launcher picked for the mission is the Delta II 7000 series by Boeing Integrated Defense Systems. This was the only possible choice of launcher that would have been able to provide the 1100 kg SC with a final C3 energy of $16.4 \frac{km^2}{s^2}$. The launch sequence consisted of a direct injection into the heliocentric orbit, following a burn sequence that lasted 57 minutes.

1.6.2 Interplanetary leg

To achieve the goal of reaching Mercury and successfully injecting into a closed orbit around the planet, a very precisely calculated sequence of gravity assists was deemed necessary.

This is since no form of propulsion could feasibly inject the SC directly into an interplanetary arc that intersects Mercury's path in such a way to make a capture at the planet possible in terms of ΔV due to technological constraints.

The final interplanetary trajectory developed by Johns Hopkins University's APL [11][4] makes use of 6 flybys before the final Mercury Orbit Injection (MOI), 1 at Earth, followed by 2 at Venus, then 3 at Mercury. This allows to significantly reduce the cost of the transfer in terms of ΔV needed to only $\approx 1100 \frac{m}{s}$, as well as in terms of mission cost and complexity of the spacecraft itself, at the expense of total transfer time.

Particular attention was placed into crafting a trajectory that would not need the spacecraft to maneuver during solar conjunctions (Sun-Earth-SC angle < 3 deg) and that would allow the SC to perform the necessary Deep Space Maneuvers (DSMs) in an orientation that allowed the heat shield to be pointed sunward when the probe is closer than 0.85AU from the Sun, thus protecting the sensitive components onboard from direct exposure to the Sun's heat and radiation. Because of its inner complexity, the trajectory was quite sensitive to the departure date, reason why three launch opportunities were found in 2004 with varying combinations of Venus, Mercury and Earth flybys; eventually the launch occurred during the last window.

1.6.3 Mercury orbit

The orbit around Mercury was chosen to be a highly elliptical one, with a minimum height above the surface of 200 km and a maximum one of almost 15200 km , an inclination of 82.5° to Mercury's equator and a low point in the orbit that was reached at a latitude of $60^\circ N$.

This was done to optimize different aspects of the mission [3][8]: this maneuver limits the propellant and ΔV that must be expended to inject into orbit, requiring 31 % of the onboard fuel reserves and a ΔV of $860 \frac{m}{s}$. This choice also leaves time for the spacecraft to cool down between perihelion passes, where heat radiated from the surface of Mercury causes an increase in total thermal flux on the SC.

The high inclination allows both to observe and study the polar regions of the planet as well as to map the whole surface of the planet.

The low periapsis leads to a higher resolution in terrain scanning, while the high apoapsis and eccentricity allow the SC to frequently pass through different strata of the magnetosphere of Mercury to study the interaction between the magnetic field of the planet and of the Sun.

The Injection burn is also planned to happen in such a way to be executed while pointing the sunshield sunward to protect the SC.

1.6.4 ΔV estimations

All gravity assists performed by Messenger during its transfer to Mercury were unpowered Fly-Bys. The ΔV cost of the transfer is mainly due to the Deep Space Maneuvers that Messenger performed between planetary encounters to adjust the trajectory ahead of the following scheduled Fly-By.

Retrieving the post-flight Keplerian elements[11][12] of the interplanetary arcs between Fly-Bys and DSMs, some of which are shown in table 1.3, it is possible to estimate the ΔV cost of each DSM as a single impulse burn by taking the norm of the difference of the velocity vector before and after the maneuver.

<i>ID</i>	<i>a</i> [km]	<i>e</i> [-]	<i>i</i> [rad]	<i>RAAN</i> [rad]	ω [rad]	θ [rad] ¹
Pre DSM-1	1.2101e8	0.2550	0.0442	2.2743	0.0365	6.1384
Post DSM-1	1.2406e8	0.2732	0.0450	2.2720	0.0315	6.1455
Pre DSM-2	8.0570e7	0.3836	0.1182	0.8780	6.2201	2.5754
Post DSM-2	7.9949e7	0.3917	0.1187	0.8751	6.2071	2.5914
Pre DSM-4	6.9753e7	0.3516	0.1222	0.8435	0.3393	2.9851
Post DSM-4	7.0308e7	0.3413	0.1221	0.8433	0.3468	2.9781

Table 1.3: Interplanetary leg keplerian elements

This analysis shows that the impulse approximation is quite precise as a first estimate of the ΔV cost for this phase of the mission as reported in Tab.1.4.

Maneuver	DSM-1	DSM-2	DSM-4
Computed $\Delta V[\frac{m}{s}]$	313.6	227.6	246.3
Real $\Delta V[\frac{m}{s}]$	315.6	227.4	246.8

Table 1.4: Calculated vs real costs of some DSMs

The accuracy of the previous results is not surprising since the team computed the ΔV using the post-flight Keplerian elements related to the points right before and after the manoeuvre reported in Tab.1.3.

Performing simulations for the ΔV cost of the launch phase or the Mercury Injection Orbit (MOI) results in some misleading results, as those maneuvers are much longer in duration and as such the hypothesis of impulsive burn cannot be applied. In particular, the calculated MOI burn is $295.9 \frac{m}{s}$, where in reality the correct value is $861.7 \frac{m}{s}$. This difference is to be expected due to the movement of the spacecraft along its hyperbolic trajectory around Mercury during the $\approx 885 s$ burn.

A more refined model is needed to correctly estimate the cost of this maneuver.

1.6.5 Δt estimations

An estimation on the time required for the interplanetary leg of the mission can be retrieved by analyzing the Keplerian elements [11] of the various legs of the transfer. Computing the time needed to travel through all of them under the hypothesis of unperturbed Keplerian motion it is possible to get estimates for the different arcs that match closely with the real timeline of the mission.

Interplanetary leg	Launch - Earth FB	Earth FB - Venus FB1	Mercury FB1 - Mercury FB2	Total time
Computed $\Delta t[days]$	366.47	448.78	266.94	2444.4
Real $\Delta t[days]$	364.49	447.56	265.57	2417.7

Table 1.5: Calculated vs real transfer times for some interplanetary legs

¹ θ refers to the true anomaly

Assignment 2: Propulsion subsystem

2.1 Architecture

MESSENGER's propulsion system consists in a pressurized bipropellant, dual-mode system feeding a set of 17 thrusters, in order to fulfill mission's requests in terms of Δv changes. The bipropellant mode uses hydrazine (N_2H_4) as fuel and nitrogen tetroxide (N_2O_4) as oxidizer. On the other hand, monopropellant mode uses hydrazine. Down in Figure 2.1 is the subsystem's arrangement:

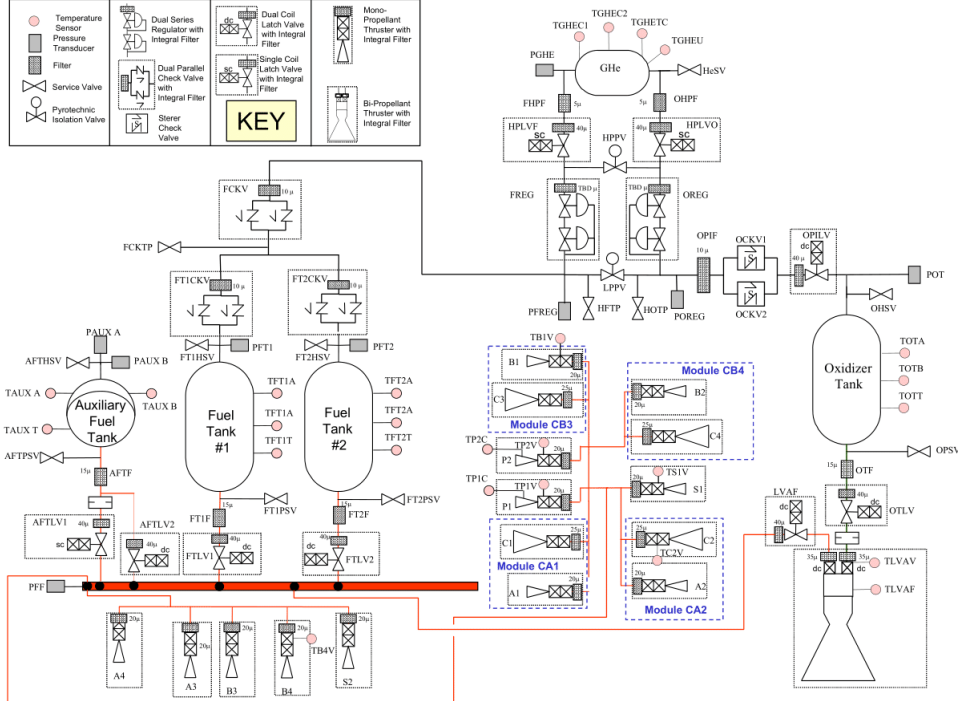


Figure 2.1: Schematics of the propulsion subsystem

2.1.1 Tanks

The two fuel tanks storing approximately 365.34 kg of fuel, and the oxidizer tank storing 231.61 kg of oxidizer, are positioned symmetrically with respect to the spacecraft's centerline in order to easily maintain mass control during the firings. Both the fuel and the oxidizer tanks are included in a pressure-fed system: they are pressurized with helium, which is contained in a high-pressure tank at approximately $232,7 \text{ bar}$. The fuel tanks are kept at around 19.5 bar during the firing, while the operating pressure of the oxidizer tank is 19.1 bar . The fuel tanks are pressurized before firing. An auxiliary refillable fuel tank is mounted on the side of the spacecraft; however, this is not linked with the helium tank and operates in a blowdown mode, between 20.7 and $7,58 \text{ bar}$.

Choosing a pressure-fed solution for the main tanks and a blowdown for the auxiliary one has several advantages: despite the need to pressurize the tanks, this architecture allows the system to be lighter with respect to a pump-fed system, which is way more complex and requires more space to be implemented in the spacecraft, and would increase the total mass to suboptimal levels. Furthermore, this comes with acceptable properties in terms of performance, while the use of a purely blowdown system would lead to lower and lower engine efficiencies as the propellant load is used and its pressure decreased.

2.1.2 Propellant supply

Once the pressurization system is activated, in order to reach the tanks, the pressurized helium must pass through filters, series of redundant regulators, latch valves, check valves and cross strapping pyro valves, whose role is crucial since they provide the apparatus cross strapping capability in case of latch valves or regulators failure. Pipes and valves link the main and the auxiliary fuel tanks for operations of refilling/dRAINing. The propellants flow from the pressurized tanks to the engines or to the auxiliary tank by following the pressure gradient.

2.1.3 Thrusters

The set of 17 thrusters includes three different thruster types, with respect to the force they shall provide to the spacecraft. Figure 2.2 shows the spatial configuration of the thrusters:

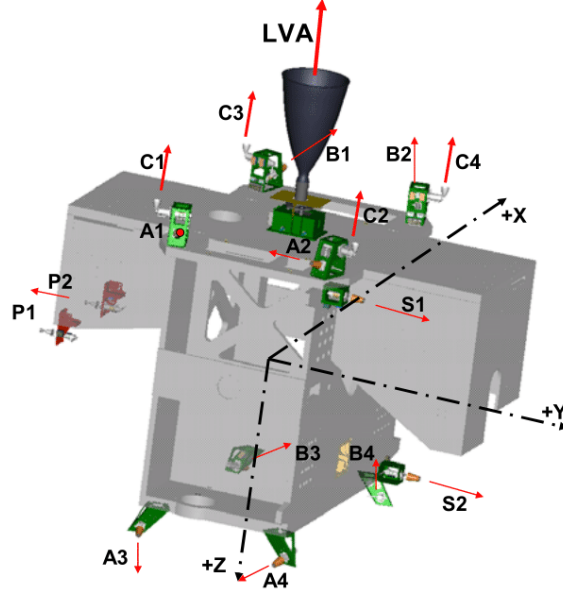


Figure 2.2: Arrangement of thrusters

The **LVA** (Large Velocity Adjuster) thruster is the bipropellant portion of the system and provides a thrust level of 667 N and a specific impulse of 316 s, in the -Z direction; it is the most powerful engine of the spacecraft, granting major Δv changes. Four monopropellant thrusters disposed in the -Z side (identified as **C**-thrusters) provide a force of 22 N and a specific impulse of 230 s each. Finally, twelve monopropellant engines grant a force of 4.4 N and a specific impulse of 220 s each. More specifically, eight thrusters (**A** in the +X side and **B** in the -X side) are disposed in double canted sets of four for redundant attitude control on the three axes, in modules together with the C-thrusters, even though they yield force in different directions. The remaining four motors (**S** in the +Y side and **P** in the -Y side) are meant to provide velocity changes in the sunward direction (S-thrusters) or in the away-from-the-sun direction (P-thrusters).

The spatial configuration of the A, B, S, and P motors ensures that no maneuver requires a null command, limiting the waste of propellant. Furthermore, it is possible to split the required thrust between opposing thrusters on opposite sides of the spacecraft in order to cancel out any residual force. That allows to have a finer attitude control and to use the minimum number of burns to complete a specific task.

2.2 Primary and Secondary Propulsion

The propulsion system's duty is to provide MESSENGER with the ΔV requested throughout its operational lifetime in order to fulfill its mission. Two types of propulsion are identified:

- **Primary propulsion:** orbital changes and correction;
- **Secondary propulsion:** station-keeping and attitude control.

Table 2.1 illustrates the different functions of the different engines.

Thruster	Charge	Tasks
LVA	Primary propulsion	Operations requiring the highest ΔV budget
C	Primary propulsion	Thrust vector steering forces during LVA burns; provide propulsion for smaller ΔV maneuvers
A, B, S, P	Secondary propulsion	Fine attitude control burns; small ΔV burns; momentum management

Table 2.1: *Thrusters' tasks*

2.3 Justification of the selected propulsion type

Before explaining the functioning of each mode, the first maneuver required by the spacecraft after being deployed is the **Detumbling**. All eight A and B attitude control system thrusters are fired to stabilize the spacecraft. The maneuver lasted for a total of 160 seconds where the goal was to spend the least possible amount of ΔV . After completion of thruster firings and system safing, cruise phase propulsion system heaters were enabled and therefore the spacecraft switched to Cruise Phase Mode.

2.3.1 Operations / Phases

The Propulsion System has four operational modes: a cruise phase mode and three thruster operational modes.

The **Cruise Phase Mode**, is the only phase that does not require the use of thrusters to perform a maneuver. In this mode, the propulsion subsystem temperature is maintained within its operational range using heaters.

The **Mode 1** is characterized by the use of the auxiliary fuel tank for the whole maneuver. In this mode, either the 22N or the 4.4N monopropellant thrusters are operated in blowdown configuration to provide small- ΔV trajectory correction maneuvers or momentum dumps.

Mode-1 maneuvers execute in two segments: main burn and tweak. The main burn segment is used to achieve the ΔV target, and the tweak segment follows to maintain spacecraft attitude. Momentum dumps are executed only as a tweak segment because they are not meant to impart any net ΔV . These fine adjustments justify the need of the 4.4N monopropellant thrusters. At the end of the tweak, the propellant system's work is over and the attitude control is taken over by the reaction wheels. As a matter of fact, using these thrusters is also justified in order to desaturate the reaction wheels if needed.

The **Mode 2** is characterized by the use of both the 4.4N and 22N monopropellant thrusters pressure-fed from the main fuel tanks as the primary propellant source.

Mode-2 maneuvers execute in three segments: settle burn, main burn, and tweak. Given that the main propellant tanks do not have propellant-management devices, a monopropellant thruster settling burn must be executed from the auxiliary tank to move the propellant to the main tank outlet before it can be accessed. To provide the necessary direction settling force, the A1, A2, B1, and B2 top deck 4.4N thrusters are nominally fired for 15 seconds. For the main burn, the high-pressure fuel latch valve is opened, and the 22N thrusters or 4.4N thrusters oriented in the $-z$ direction are operated using one of the pressurized main fuel tanks. As with a Mode 1 maneuver, the main burn segment ends when the ΔV target is achieved, and the tweak segment is used to keep the spacecraft attitude. Since both auxiliary fuel tank latch valves remain open for the entirety of the maneuver, the auxiliary tank is refilled while the main burn proceeds. Throughout the maneuver, attitude control is accomplished by off-pulsing the primary thrusters and on-pulsing 4.4N thrusters.

The **Mode 3** is used for large ΔV maneuvers and uses the bipropellant LVA thruster, which is pressure-fed from the main fuel and oxidizer tanks. This N_2H_4/N_2O_4 - based thruster is vital in order to provide the spacecraft with the required Deep Space Maneuvers already planned during the numerous interplanetary legs but also to perform the Mercury Orbit Insertion which requires a huge amount of ΔV .

Mode 3 maneuvers execute in five segments: settle burn, refill burn, main burn, trim burn and tweak. The settle and tweak segments are the same as those of a Mode-2 maneuver. The settle burn is followed by a separate refill segment. During this segment, the top deck 4.4N thrusters are fed by a main fuel tank and fire for a predetermined duration to refill the auxiliary tank. For the main burn, all three latch valves upstream of the main propellant tanks are opened, and the LVA is operated using the pressurized main fuel and oxidizer tanks as the primary propellant sources. The four 22N thrusters are on-pulsed for LVA thrust vector control, and the 4.4N thrusters are on-pulsed for fine attitude control. After the LVA has achieved a certain percentage of the required ΔV , the system transitions to the trim segment. During trim, the 22N thrusters are used to ensure a more precise completion of the required ΔV . To maintain a manageable spacecraft center of mass, the main fuel tanks are switched every 20 seconds during the main and trim burn segments by opening and closing their outlet latch valves. Otherwise, the thrust vector will generate a net torque that the 22N thrusters are not able to control.

2.3.2 DeltaV budget breakdown

The ΔV budget is split into different type of maneuvers, namely :

- Detumbling (DET)
- Mercury Orbit Injection (MOI)
- Deep Space Maneuvers (DSM)
- Orbit Correction Maneuvers (OCM)
- Trajectory Correction Maneuvers (TCM)
- Momentum Dumps (MD)

The very first maneuver to be implemented was the detumbling in order to stabilize the spacecraft.

	ΔV [m/s]	Date	Mode	Thrusters Used
DET	0.46	3 Aug 2004	1	A,B

Table 2.2: *Detumbling*

To begin with, the DSM are Trajectory Control Maneuvers (TCM) with the largest velocity change. They were done within the different interplanetary legs of the flight of MESSENGER all using Mode 3.

	ΔV [m/s]	Date	Mode	Thrusters Used
DSM1	315.6	12 Dec 2005	3	LVA
DSM2	227.4	17 Oct 2007	3	LVA,B
DSM3	72.2	19 Mar 2008	3	LVA
DSM4	246.8	4 Dec 2008	3	LVA
DSM5	177.8	24 Nov 2009	3	LVA

Table 2.3: *Deep Space Maneuvers*

Contingency maneuvers TCM-4, TCM-7, TCM-8, TCM-14, and TCM-17 were never implemented due to the achievement of sufficient accuracy with the prior TCMs. After TCM-19, only the aforementioned DSM3, DSM4 and DSM5 were required before the MOI. Future trajectory corrections were made using solar sailing techniques by orienting the sunshade and solar panels in an appropriate way.

	ΔV [m/s]	Date	Mode	Thrusters Used
TCM1	17.9	24 Aug 2004	2	C
TCM2	4.6	24 Sep 2004	2	C
TCM3	3.2	18 Nov 2004	2	C
TCM5	1.1	23 Jun 2005	1	S
TCM6	0.2	21 Jul 2005	1	P
TCM10	1.3	22 Feb 2006	1	B
TCM11	2.3	12 Sep 2006	2	C,S
TCM12	0.5	5 Oct 2006	1	B
TCM13	35.7	2 Dec 2006	3	LVA,P
TCM15	0.6	25 Apr 2007	1	B
TCM16	0.2	25 May 2007	1	B
TCM19	1.1	19 Dec 2007	1	B

Table 2.4: *Trajectory Correction Maneuvers*

About 31% of the spacecraft's propellant was required for Mercury orbit insertion (MOI) in order to place the spacecraft into its primary science orbit around Mercury. MESSENGER's thrusters slowed the spacecraft by 861.7 meters per second. As the spacecraft approached Mercury, the largest thruster was pointed close to the forward velocity direction of the spacecraft. The maneuver lasted about 15 minutes.

	ΔV [m/s]	Date	Mode	Thrusters Used
MOI	861.7	18 Mar 2011	3	LVA

Table 2.5: *Mercury Orbit Injection*

Already in Mercury's science orbit, the spacecraft needed to counteract the effects of the solar gravity which was acting on the spacecraft's orbit. Therefore, 4 Orbit Correction Maneuvers (OCM1, OCM3, OCM5, OCM6) were implemented at the apogee of the orbit to place MESSENGER with a minimum perigee distance of 200 km. The second and fourth maneuvers after MOI increased the orbit period to about 12 hours by speeding up the spacecraft near its closest distance from Mercury.

During the first extended mission of MESSENGER which started on 18 March 2012, two orbit-correction maneuvers lowered the spacecraft's orbit period from 11.6 hours to 8 hours finally depleting the oxidizer reserves by using the LVA thruster (OCM7). During the second extended mission of MESSENGER which began on 18 March 2013, four OCMs targeted a minimum altitude of 25km and 15km for the last OCM. During the last extended mission of MESSENGER which lasted 6 weeks until the crash, 7 OCMs targeted a specific minimum altitude. OCMs 13, 14, and 15 consumed nearly all remaining usable hydrazine from the auxiliary fuel tank. The final two OC maneuvers raised the spacecraft's minimum altitude above Mercury just enough to ensure impact onto Mercury during an orbit for which coverage by one of DSN's large antennas had been scheduled. Such a downlink arrangement enabled the transmission to Earth of nearly all images and science data remaining on the spacecraft recorder.

The final impact occurred the 30 April 2015.

	ΔV [m/s]	Date		ΔV [m/s]	Date
OCM1	27.8	15 Jun 2011	OCM11	19.3	24 Oct 2014
OCM2	4.0	26 Jul 2011	OCM12	9.6	21 Jan 2015
OCM3	24.9	7 Sep 2011	OCM13	3.1	18 Mar 2015
OCM4	4.1	24 Oct 2011	OCM14	3.1	2 Apr 2015
OCM5	22.2	5 Dec 2011	OCM15	1.8	6 Apr 2015
OCM6	19.2	3 Mar 2012	OCM15A	1.8	8 Apr 2015
OCM7	53.3	16 Apr 2012	OCM16	1.0	14 Apr 2015
OCM8	31.4	20 Apr 2012	OCM17	1.5	24 Apr 2015
OCM9	5.0	17 Jun 2014	OCM18	0.4	28 Apr 2015
OCM10	8.6	12 Sep 2014			

Table 2.6: *Orbit Correction Maneuvers*

Furthermore, there were a total of 181 Momentum Dumps, which include 1 Autonomous Momentum Dump (AMD) and 180 Commanded Momentum Dumps (CMD). Since they are Attitude Control Maneuvers, the ΔV they provide is negligible, very close to 0.00 m/s. They are all operated through Mode 1 thanks to the 4.4N attitude control system thrusters A and B.

The total ΔV budget adding everything together is of 2213.17 m/s.

2.4 Reverse Sizing

2.4.1 Propellant selection and masses

The propellant couple (hydrazine and nitrogen tetroxide) was selected thanks to its ability to guarantee high thrust when used as bipropellant, but also low thrust (needed for small maneuvers and fine adjustments) when used hydrazine as monopropellant. This solution allows the primary and secondary propulsion to use the same propellant, reducing the complexity and total mass of the system. Vacuum specific impulse in both bipropellant and monopropellant mode satisfies the requirements. Hydrazine and nitrogen tetroxide are also hypergolic, which grants reliable and repeatable ignition, high density and storable, all fundamental aspects

when considering a long space mission. Furthermore this propellant couple has been tested and successfully used for many previous missions.

The total mass of the propellant needed for the mission has been calculated starting from the data shown in Table (2.7).

$I_{sp,bi}$ [s]	$I_{sp,mono}$ [s]	Δv [m/s]	m_s [kg]	O/F
316	230	2300	507.9	0.85

Table 2.7: Initial data

Knowing that $\approx 90\%$ of the Δv has been assigned to the primary propulsion, a weighted average specific impulse can be obtained. It can be then used in the rocket equation to calculate to total propellant mass:

$$m_p = m_s \cdot \left(\exp\left(\frac{\Delta v}{g_0 I_{sp,avg}}\right) - 1 \right) \cdot 1.02 \quad (2.1)$$

A margin of 2% has to be added to account for propellant residuals. The masses of fuel and oxidizer are found, considering that $\approx 90\%$ of the mass has been assigned to the bi-propellant motor.

$$m_{f,mono} = 0.1 \cdot m_p \quad m_{f,bi} = \frac{0.9 \cdot m_p}{1 + O/F} \quad m_{ox} = 0.9 \cdot m_p - m_{f,bi} \quad (2.2)$$

Results compared to the real messenger data are shown in Table (2.8)

-	m_p [kg]	m_f [kg]	m_{ox} [kg]
Reverse sizing	593.84	348.63	245.20
Real	596.95	365.34	231.61

Table 2.8: Propellant mass sizing results

The slight discrepancy may be explained by the need for a higher safety factor on the propellant mass of the monopropellant thrusters, such as the 100% safety factor on the predicted station keeping propellant needed.

2.4.2 Tanks sizing

In order to decide the number of tanks needed by the mission, the volume of propellant has to be analyzed. In this case the total volume of fuel required is more than double the volume of oxidizer. The best solution is then to use three main identical tanks (to minimize tank qualification, tooling and manufacturing costs), two for hydrazine and one for nitrogen tetroxide, and one smaller auxiliary tank filled with hydrazine. The use of an auxiliary tank is very effective for minimizing the mass and complexity of the three bigger tanks, since it allows to use in-line trap propellant management devices and vortex baffles in place of diaphragms. Small, 2 m/s, monopropellant settling burns use the auxiliary fuel tank, which has an elastomeric diaphragm, in blowdown mode prior to each bipropellant burn to settle the propellant at the tank outlets.

Propellant tanks need to be able to withstand the high pressures required, while minimizing their weight. For this purpose the best shape would be that of a sphere, which works perfectly for small sized tanks, like the auxiliary tank. For bigger tanks though, this option is very space inefficient, therefore the best choice becomes a cylindrical shape with two half domes at the end, used for the three main tanks and for the pressurizer tank. Material selection is of paramount importance in order to minimize the mass and to avoid tank corrosion and propellant decomposition. The lightest option for the pressurant tank is a titanium-lined composite over-wrapped leak-before-burst pressure vessel (COPV), an already flight-proven technology for helium tanks. Its use would not be safe for the propellant tanks, due to a lack of testing for pressure-fed systems. Instead, 6Al-4V titanium has been used, given its proven reliability and compatibility with both fuel and oxidizer, as well as its low density and high tensile strength.

In order to find the dimensions of the main tanks, 25% of unusable volume has been added to the volume of propellant. Then the value of the tanks radius has to be chosen, considering the trade-off between space

efficiency and mass. For the purpose of this paper, the radius has been assumed to be 559 mm, equal to the real tank radius. The length, thickness of the cylindrical part and thickness of the hemispherical part of the tank can then be calculated as:

$$\text{length} = \frac{V - \frac{4}{3}\pi r^3}{\pi r^2} + 2r \quad th_{cyl} = \frac{2P \cdot r}{\sigma} \quad th_{sph} = \frac{P \cdot r}{\sigma} \quad (2.3)$$

Where r is the internal radius of the tank, P is the pressure inside the tank and σ is the yield stress of the material. A safety factor of 2 has been considered in the calculation of the thickness.

The mass is now found, and the results are shown in Table (2.9).

-	length [mm]	th _{cyl} [mm]	th _{sph} [mm]	m _{tank} [kg]
Reverse sizing	998	1.2	0.6	6.6
Real	1041	1	0.5	9.1

Table 2.9: Tank sizing results

The difference in mass can be explained by noting that, while sizing the tank, vortex suppressors, baffles and inlet/outlet ports haven't been considered.

2.4.3 Pressurant selection and masses

The selected pressurant is Helium, very lightweight and inert, thus non-reactive. It also has been widely used for this purpose, proving its reliability.

Given the long operating time, an isothermal expansion (at 293K) of the pressurising helium is modeled. Densities of the propellants are retrieved from literature and are $\rho_{Fu} = 1004.5 \frac{\text{kg}}{\text{m}^3}$ and $\rho_{Ox} = 1450 \frac{\text{kg}}{\text{m}^3}$. Density of helium is computed considering it a perfect gas through the state equation.

Helium initial storage pressure is known (i.e. 232, 7 bar), and the propellants tanks are modeled as being pressurized at the pressure level required before engine ignition (i.e. $P_{tank} = 19.3$ bar).

An extra 20% of pressurant is taken to account for a safety margin.

$$V_{He} = \frac{(V_{Ox} + V_{Fu}) \cdot P_{tank}}{P_{He,initial}} \cdot 1.2 \quad (2.4) \qquad m_{He} = V_{He} \cdot \rho_{He} \quad (2.5)$$

	m _{He} [kg]	V _{He} [m ³]
Reverse sizing	2.459	0.0642
Real	2.295	0.0672

Table 2.10: Pressurization subsystem sizing

2.4.4 Feeding subsystem sizing

In order to retrieve the pressure in the tanks, nominal chamber pressures of 16 bar and 10.9 bar have been considered respectively for the main motor and for the 22N secondary motor (the highest nominal pressure one). Then using typical values of $10 \frac{\text{m}}{\text{s}}$ for the flow velocities and 0.2 P_c for the pressure drop in the injector, the following results can be obtained (Table 2.11).

-	Oxidizer tank pressure [bar]	Fuel tank pressure [bar]	Auxiliary tank pressure [bar]
Reverse sizing	19.8	19.6	13.5
Real	19.5	19.1	20.7-7.58

Table 2.11: Feed system sizing

The auxiliary tank seems to be unable to satisfy the motor pressure requirements in some scenarios, but it has to be noted that, in order for the pressure to fall to the lower range limit, the tank has to be completely empty. Moreover the required pressure has been calculated using the motor's nominal pressure only, while in reality it is able to function with much lower pressures.

Assignment 3: TTMTTC subsystem

3.1 TTMTTC Architecture

The MESSENGER Radio Frequency (RF) telecommunications system is based upon a complete and redundant, yet not undue configuration of antennas, X-Band transponders and amplifiers both for uplink, downlink and radiometric tracking data.

The choice of frequency and band for the mission was dictated by the available operating frequencies of NASA's DSN, which can operate in the S-Band (2.1 GHz Uplink, 2.3 GHz Downlink), X-Band (7.2 GHz Uplink, 8.4 GHz Downlink), and Ka-Band (34.2 GHz Uplink, 32.0 GHz Downlink).

Given the high required datarate of the mission, the S-Band was not chosen as it could not satisfy the needs of the mission in terms of datarate and it is in general used for missions traveling to the outer planets of the Solar system thanks to the lower free space losses, or for missions where achieving a high bitrate is not a concern. Moreover, technologies based on S-band frequencies are more mature indeed, their extensive use has made these frequencies overcrowded, this implies that it is more difficult to obtain the licence for transmitting in the S-band. Since this band deals with lower frequencies, it requires bigger antennas that can be difficult to be integrated in the spacecraft: notice that the maximum frequency allowed in the S-band is approximately half the minimum frequency available in the X-band: this implies that antennas shall at least double in dimension to grant the same performances.

At the same time, the Ka-Band would allow for higher bandwidth and datarate but its higher frequency would lead to high free space losses due to the high maximum distances achieved during the mission's lifetime, resulting in an increased required transmitted power or gain that on the other hand, would create a narrower beam resulting in increased misalignment losses; it will also be very strongly affected by rain and the atmosphere.

On the other hand, the frequencies used in the X-Band, lower than the Ka-band but higher than the S-band, show a very resilient behaviour with respect to the atmospheric phenomena allowing for much reliable links, while guaranteeing sufficient datarate for the scientific needs of the mission and a manageable transmitter power request[31][32].

Eventually some considerations about the Doppler effect can be done[33], in particular:

$$f_D = \frac{v_r \cdot f_0}{c} \cdot \cos(\alpha) \rightarrow \max(f_D) = \frac{v_r \cdot f_0}{c} \quad (3.1)$$

where f_D is the received frequency and f_0 is the transmitted frequency. Notice that the frequency shift is proportional to the carrier frequency, larger shifts require antennas able to receive in a greater bandwidth in order to not lose the signal.

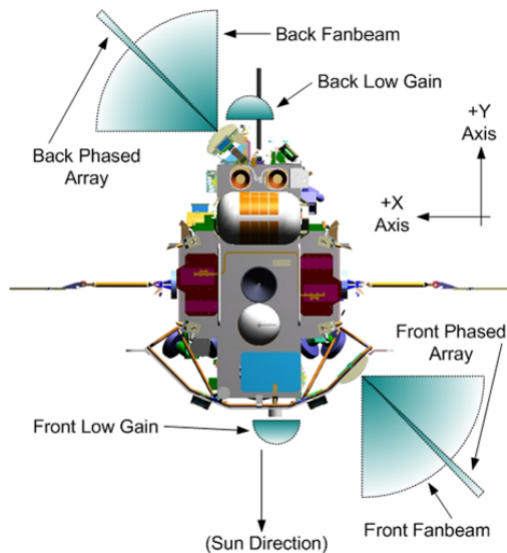
The final RF subsystem configuration for the antennas consists of: two High-Gain Waveguide-Based Phased Array antennas, two Medium-Gain Fanbeam Antennas, and four Hemispherical Low-Gain Antennas[22].

- The two identical lightweight, High-gain, Waveguide-Based Phased Arrays (18 cm x 76 cm) (PAAs) are used for high bit-rate science downlink. These electronically steerable antennas are mounted on opposite sides of the spacecraft. Rotating the probe on the Y-axis, they are able to cover each one one full hemisphere, with a scanning capability of +/- 60° in the XY-plane of the spacecraft, transmitting at 8.4 GHz. They are not used for reception.
They are placed respectively, one on the sunshade and the other on the back of the spacecraft, one facing Sun, the other in the opposite direction eliminating the need for a heavy and complex mechanically gimbaled high-gain antenna (HGA). This system reduces the weight and improve overall high temperature resilience creating a low risk solution.
- The two Medium-Gain Fanbeam Antennas (MGA) are used for commanding and low bit-rate downlink purposes. They are characterized by a beamwidth of 90°, a transmitting frequency of 8.4 GHz and receiving one of 7.2 GHz. Each of these antennas provides coverage in diametrically opposite quadrants of the plane normal to the sunshade, full 360° coverage in this plane is accomplished by rotating the spacecraft along the Spacecraft-Sun line, allowing for constant view of Earth.
- The four hemispherical Low-Gain Antennas (LGA) are used in burn mode, emergency as well as near-Earth communications. They provide coverage in all directions, without the necessity of rotating the spacecraft in one particular direction. This aspect furthermore enables constant communications while keeping the sunshade pointed in the Sun direction. These antennas are able to transmit at 8.4 GHz and receive at 7.2 GHz.

All the selected antennas have no mechanical components, which could fail in the challenging thermal environment of Mercury. Thanks to this design choice the final configuration is able to work over a 350°C range in temperatures. Another peculiar aspect of this mission is that MESSENGER is exploring one of the inner planets of the solar system, closer than Earth to the Sun: this geometric constrain implies that the planet can be in every possible direction with respect to the spacecraft, requiring antenna coverage in all the possible directions. Furthermore the antennas are located at the ends of the shade to give a clear view to space for backside heat radiation.

The system is completed by a set of[22]:

- General Dynamics Small Deep Space (X-band) Transponders (SDSTs) in redundant quantity. Responsible for receiving and modulating the RF uplink signal, generating and modulating the RF downlink signal, and turning around uplinked ranging and Doppler components. Each SDST's downlink signal (only one is active at any given time) is routed via a passive hybrid coupler to both solid-state power amplifiers (SSPAs).
- Solid-State Power Amplifiers (SSPAs), at least one for each phased-array antenna. A Solid-State solution was preferred over Travelling Wave Tube Amplifier (TWTA) because of the reduced weight and the sufficient output power radio, despite being smaller compared with the one provided by TWTA. The lower efficiency is not a concern for the mission, as at the distance of Mercury solar power is abundant but weight is a critical element of the design process. Each SSPA can be in one of four modes: "distributed front," "distributed back," "lumped," and "off." The "distributed" modes of the SSPAs feed the RF downlink signal to either the front or the back PAA; the "lumped" mode of the SSPA feeds the RF downlink signal, via the two RF switch assemblies, to the fanbeam antenna or the LGAs. In the "distributed" mode, the RF signal is split in eight ways and routed to eight "stick amplifiers." Each stick amplifier consists of a four-bit phase shifter (that controls the steering of the phased-array antenna beam), a small-signal amplifier, a driver amplifier, a power amplifier, and an isolator. The output power of each stick amplifier is approximately 34 dBm; in a distributed mode, a total of four sticks are operational per SSPA, yielding an output power of approximately 40 dBm. The "lumped" mode of the amplifier offers a 40 dBm power output for the fanbeam and low-gain antennas.



3.2 Mission phases and operations

Contact strategy for the MESSENGER mission is dependant on a variety of factors, such as distance between spacecraft and ground station, main disturbances, and type and rate of data to be transferred to and from the spacecraft at each mission phase[22].

- During the launch and early phase of mission, uplink and downlink are expected to be at least 31.25 bps and 1000 bps respectively.

The small distance from Earth is not imposing peculiar solutions regarding the signal reception, nevertheless connection with the spacecraft cannot afford to be lost. Thus, all the four LGAs are on, providing omnidirectional coverage, being in fact less susceptible than high gain antennas to loss of signal. Moreover, data to be transmitted are expected to be less than the other phases, not representing the focus of this phase.

- The cruise phase is designed for minimizing human intervention on the spacecraft control thus preserving resources. Orbit determination during the cruise phase relies primarily on the Deep Space Network (DSN) Doppler and ranging tracking data. On approach to the Venus and Mercury flybys, these data will be augmented with both DSN Delta Differential One-Way Ranging (ΔDOR) and optical navigation measurements. The solution for signal receiving and spacecraft tracking is a 34 m DSN antenna.
- In the orbital period the primary focus shifts on science data to be collected and transmitted. During on-orbit operations rotation about the Sun line is required to accommodate instrument viewing, since the instrument-view direction is normal to the spacecraft-Sun line and opposite the LVA direction (the direction of the main thruster, Large Velocity Adjust). Although thermal requirements are always met high-rate downlink communications are not maintained during the rotation periods. A 34 m DSN antenna is used for the receiving with an average of 6.5 hours time window per day. Once in Mercury orbit, the RF configuration will route the uplink through the most favorable fanbeam antenna and the downlink via a phased array for high-rate data-transmission passes. LGAs are not normally on during this phase. The total amount of scientific data retrieved in this phase is expected to be more than 100 Gb during the first year of operations.
- During both cruise and orbital operations, periods of solar conjunction precludes communications. Prior to these times, the spacecraft is placed into a safe-hold mode. No events requiring communications for ground commands occur during solar conjunction periods.
- In the case of an emergency communication, LGAs are used to withstand possible attitude malfunctioning, and so inaccurate pointing, granting 7.8 bps for uplink and 10 bps for downlink, while maintaining sunshade attitude requirements and 3 dB link margins. The use of LGAs in this phase requires the switch of ground station antenna from the DSN's 34 m parabolic antenna to the larger 70 m parabola, to guarantee adequate communication to and from the spacecraft.

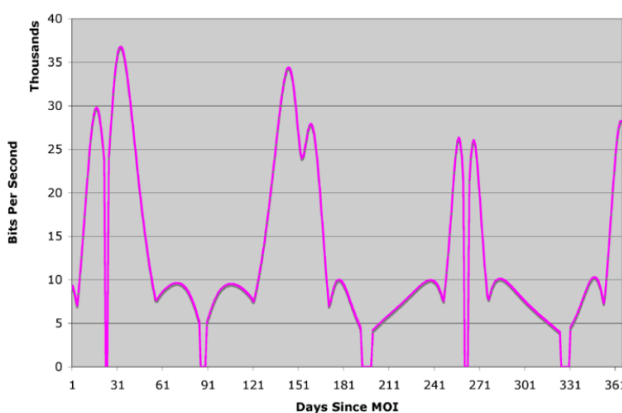


Figure 3.1: Downlink datarate

The 34 and 70 m antennas of NASA Deep Space Network are located in Goldstone, California; Madrid, Spain; and Canberra, Australia.

These three locations are spaced almost 120° apart, and thanks to the wide field of views they can achieve, guarantee full coverage of the Messenger spacecraft with at least one antenna at every moment of the mission[20].

High bit-rate is required by the presence of many on-board scientific instruments, as well as by the fact that information downlink is only available for a maximum of a 8-hour time window each day.

Information gathered by the instruments is stored onboard on internal memory before being downlinked at the following available opportunity, furthermore a data prioritization scheme will assist in managing the downlink phase.

Moreover, control signals must be considered as important as scientific data retrieval, thanks to the system configuration, described above, operators are able to send commands at 7.8 to 500 bits per second. Average datarate over the first year of the mission is in the order of 35 MB/day.

Fig. 3.1 shows the bitrate of one year during the orbital mission: peaks in the curve correspond points near Mercury inferior conjunctions while the data rate drops to zero during the inferior conjunction since it is not possible to maintain the RF link due to high disturbances connected to the solar radiation aligned with the beam. Longer segments with zero data rate instead correspond to Mercury superior conjunction.

3.3 Reverse Sizing

In this section a preliminary reverse sizing of the TTMTTC subsystem will be discussed taking into account its most important aspects.

3.3.1 Losses

The channel losses computation involves four types of contributions: free space, pointing, cable and atmospheric losses have been taken into account.

Free space losses have been computed as:

$$L_{free\ space} = 20 \cdot \log_{10} \left(\frac{c}{4 \cdot \pi \cdot f \cdot r} \right) [dB] \quad (3.2)$$

while pointing losses are:

$$\begin{cases} L_{point} = -12 \cdot \left(\frac{\eta_p}{\theta} \right)^2 [dB] \\ \theta = 63.5 \frac{c}{f \cdot D} [deg] \end{cases} \quad (3.3)$$

where: c is the speed of light, f is the wave frequency, r is the Earth-SC distance, D is the antenna diameter and η_p is the antenna pointing efficiency. **D has been assumed to be 34 m in the downlink case to be consistent with the DSN antenna dimension used considered in the literature; in the uplink case D is considered equal to $2 \cdot \lambda_{UL} = 0.0833$ m since the antenna here considered is the MGA.**

Considering that the transmission both in uplink and in downlink occurs using the X-band, atmospheric losses has been estimated as $L_{atm} = -0.045$ dB while the passive L_{cab} have been considered equal to -2 dB for the spacecraft according with the literature, and -1 dB for the DSN antennas.

The previous equations leads to the following results[23].

	Computed	Real
Downlink		
$L_{free\ space}$ [dB]	-270.0	-270.0
$L_{point+atm}$ [dB]	-0.3	-0.3
Uplink		
$L_{free\ space}$ [dB]	-268.7	NA
$L_{point+atm}$ [dB]	-0.0483	NA

Table 3.1: Losses considering Earth range = 0.6 AU

Notice that in the downlink case η_p has been estimated equal to 0.01 considering the relative error between the electronically steerable phased array antenna and the DSN antenna while, in the uplink case, the same parameter η_p has been considered equal to 0.1 since the MGA is not steerable.

3.3.2 Antennas

The analysis has been performed considering the two main different antennas mounted on Messenger: the high gain phased array (PAA), considered for downlink communications, and the medium gain fainbeam antenna (MGA) taken into account in the uplink phase.

Knowing the power of each amplifier it is possible to estimate its efficiency and the corresponding transmitted power.

$$P_{Tx} = \mu_{amp} \cdot P_{In} \quad (3.4)$$

The gain of each antenna has been estimated as follows:

$$G = 10 \cdot \log_{10} \left(\mu \cdot \left(\frac{\pi \cdot D \cdot f}{c} \right)^2 \right) [dB] \quad (3.5)$$

where:

D is the characteristic dimension of the antenna (DSN: 34 m, MGA: $2 \cdot \lambda_{UL} = 0.0833$ m)

μ is the antenna efficiency ($\mu_{para} = 0.55$, $\mu_{helix} = 0.70$)

Finally, the system noise density related to the receiving antenna is:

$$N = 10 \cdot \log_{10} (kT_s) [dB] \quad (3.6)$$

where:

k is the Boltzmann constant

T_s is the system equivalent temperature (retrieved from [23])

This process leads to the following results:

Input power [W]	Efficiency	Computed P_{tx} [W]	Real P_{tx} [W]
52	0.22	11.44	11

Table 3.2: Downlink PAA transmitted power

In this case, further losses are to be expected due to the presence of other electrical components. Each antenna gain has been computed as aforementioned except for the PAA, whose gain cannot be computed using simplified formulas, the correct value retrieved from literature [23] has been therefore accounted for the following computation.

	Computed	Real
Downlink		
$G_{Tx,HGA}$ [dB]	NA	+27.3
$G_{Rx,DSN}$ [dB]	+66.95	+68.41
Uplink		
$G_{Tx,DSN}$ [dB]	+65.59	+67.05
$G_{Rx,MGA}$ [dB]	+14.4	+15.0

Table 3.3: Antenna gains for uplink and downlink

Notice that the computation of the DSN antennas gain always underestimate the real value, this is probably due to an underestimation of the antenna efficiency in Eq3.5.

3.3.3 Link budget

The use of a $R = 1/6$ and $k = 15$ convolution encoding, together with a Reed-Solomon modulation allows for a downlink $BER \approx 10^{-5}$ with a minimum link budget of just 1 dB, a margin of 1.5 dB is then added on top of that as a safety factor; despite according with literature the margin in the link budget in a preliminary analysis shall be 3 dB, this specific encoding and modulation allows to use lower safety margins [23]; uplink instead considers $BER \approx 10^{-7}$ as commands need higher accuracy. This yields a minimum $E_b/N_0 = 2.5$ dB, with a safety margin of 3 dB.

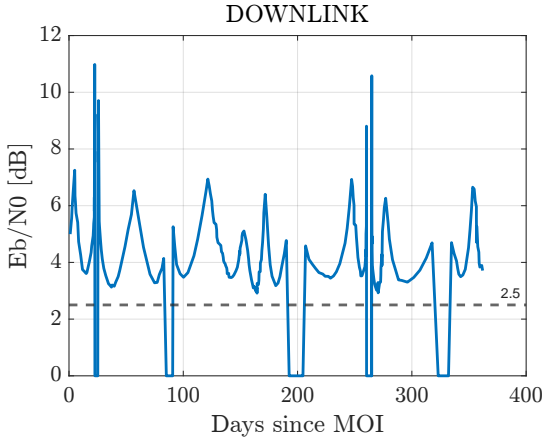
Computing the total link budget is possible by using the following formula:

$$\begin{cases} \frac{E_b}{N_0} = 10 \cdot \log_{10}(P_{Tx}) + G_{Tx} + G_{Rx} + L_{Total} - N_0 - 10 \cdot \log_{10}(R) [dB] \\ N_0 = 10 \cdot \log_{10}(kT) [dB] \\ L_{total} = L_{free\ space} + L_{point+atm} + L_{cab} [dB] \end{cases} \quad (3.7)$$

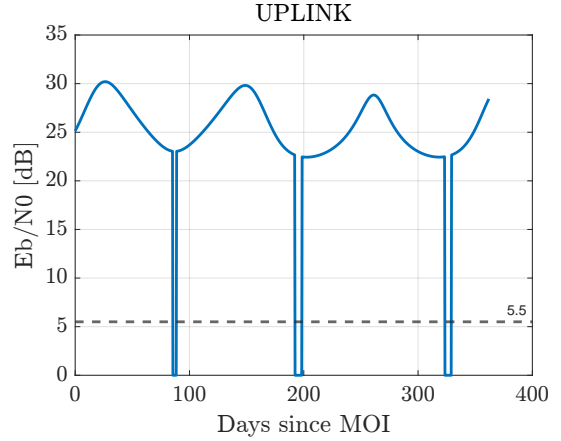
where k is the Boltzmann constant, L_{total} and the datarate R vary over time in relation to the distance between Earth and Mercury that is computed considering the ephemerides of Earth and Mercury in the corresponding period.

In particular, for the downlink analysis the datarate considered is the one obtained through Fig.3.1 while, in the uplink case the datarate has been considered as a fixed worst case scenario of 500 bps. Also the DSN antenna has been considered in the worst case scenario of 34 m diameter. All the other data necessary to fulfill the equation: have been derived through the previous computations: losses: Tab.3.1, power: Tab.3.2 and gains: Tab.3.3. The antenna temperature in the N_0 computation, has been considered equal to 21 K

for the DNS and 373 K for the spacecraft antenna since it is expected to work at high temperatures[23]. Notice that longer periods with zero link budget, since this computation is based on data from Fig 3.1, corresponds to the major conjunctions when it is impossible to establish the RF link between the Ground Station and the spacecraft.



(a) Downlink link budget



(b) Uplink link budget

The resulting link budget both for the science data downlink and telecommand uplink, appears to be satisfied for every time instant.

The bandwidth can be computed using the Shannon-Hartley theorem:

$$C = B \cdot \log_2 (1 + S/N) \quad (3.8)$$

where C is the channel capacity that is assumed to be equal to the maximum datarate required: 36.8 Mbps in downlink according with Fig.3.1, and 500 bps in uplink representing a worst case scenario. The Signal over Noise ratio (S/N) is required to be equal to 13 dB according with standard literature for a preliminary sizing. The required bandwidth results to be equal to 8.38 MHz in downlink and 114 Hz in uplink. Considering that the frequency separation between channels in the X-Band is equal to 1.358 MHz in downlink and 1.173 MHz in uplink [31], the required downlink bandwidth imposes either to use more contiguous channels or to increase the requested S/N and the corresponding transmission power according to the formula $SNR = P_{carrier} - N0 - 10 \cdot \log_{10} (B) \text{ [dB]}$.

Assignment 4: AOCS subsystem

4.1 Architecture

The MESSENGER spacecraft is a 3-axis stabilized spacecraft that uses reaction wheels and thrusters for attitude control. The combination of reaction wheels and thrusters allowed MESSENGER to achieve precise attitude control throughout its mission. The reaction wheels provided continuous and precise control over the spacecraft's attitude, while the thrusters offered additional maneuvering capabilities when larger attitude changes or orbital adjustments were required.

It's important to note that MESSENGER's attitude control system was a complex and integrated subsystem, incorporating various sensors, algorithms, and control mechanisms to ensure accurate and stable attitude control. The actuators, such as the reaction wheels and thrusters, were key components of this system, working in coordination with the spacecraft's guidance and control algorithms to maintain the desired orientation and stability in space. The set of sensors consists of star trackers, digital Sun sensors, and an inertial measurement unit. Solar panels provide electric power to the spacecraft, and a heat-resistant and reflective sunshield colored in white protects the spacecraft from the extreme thermal conditions encountered close to the Sun at a distance of less than 0.85 AU. The spacecraft body axes and selected component locations are shown in the following figure.

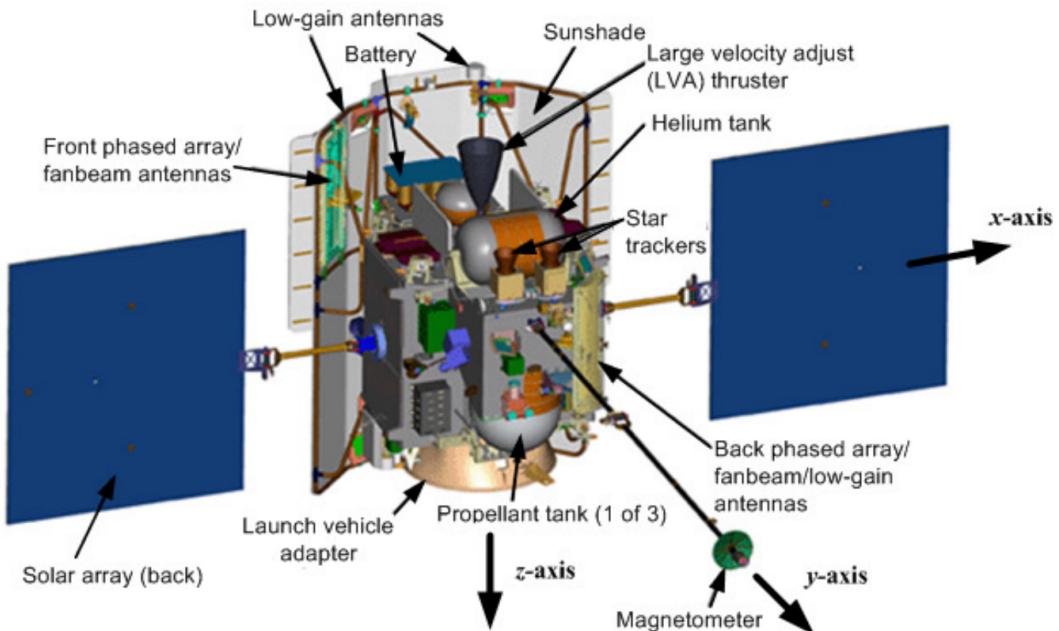


Figure 4.1: Messenger's Components and body frame

The MESSENGER guidance and control subsystem maintains spacecraft attitude and executes propulsive maneuvers for spacecraft trajectory control. Software algorithms run in the Main Processor (MP) to coordinate data processing and commanding of sensors and actuators to maintain a 3-axis stabilized spacecraft and to implement desired velocity changes.

The system enforces two attitude safety constraints :

- Sun keep-in (SKI) constraint that keeps the sunshade pointed towards the Sun to protect the spacecraft bus from extreme heat and radiation. Maintaining that specific sunshade orientation for the entire orbital mission poses an important constraint to the spacecraft's attitude.
- The hot-pole keep-out constraint protects components on the top deck of the spacecraft from additional thermal extreme temperatures due to re-radiation of sunlight from the surface of Mercury once in orbit.

4.1.1 Sensors

The sensor set consists of star trackers, an inertial measurement unit, and sun sensors. Inertial attitude reference is provided by two autonomous star trackers from Galileo Avionica, both of which are mounted on

the top deck looking out along the $-Z$ axis. They are placed in that specific location in order to avoid the Sun in its Field Of View. They have a total mass of 6.37 kg, including baffles. Each uses a maximum of 12.3 W in the normal tracking mode. The trackers do image processing to identify star patterns internally, and the attitude solution in the form of quaternion and rate is output to the flight software.

MESSENGER also carries a set of Adcole Digital Sun sensors (DSS) to provide Sun-relative attitude knowledge if there is a failure in the primary attitude sensors. Two separate Sun sensor systems consist of a DSS electronics box connected to three DSS heads, two of which are located on opposite corners of the sunshade and one on the back of the spacecraft.

	Name	FOV [°]	Number
Star Tracker	Galileo Avionica A-STR	± 16.4	2
Sun Sensor	Adcole Maryland Aerospace	± 64	3

Table 4.1: *Reaction Wheels*

Spacecraft rotation rates and translational accelerations are provided by a Northrop-Grumman Scalable Space Inertial Reference Unit IMU with four Hemispherical Resonance Gyroscopes (HRG) and Honeywell QA-3000 accelerometers. This IMU is well suited for the application, as the mission requires 3-axis stabilisation and the four gyros and accelerometers allow for such capability while also ensuring some level of redundancy in case of a single component failure. More specifically, the HRG is composed by an outer shell, a vibrating hemispherical resonator and an inner shell: because of the simple hardware and of the absence of moving parts, HRG is highly reliable. Moreover, all the parts are made of fused quartz which is naturally hardened by radiation, making them intrinsically immune to the harsh space environment and well-suited for a long-term space mission. Furthermore, HRG's advantages include a really low angle random walk and power dissipation, low noise and a compact and fault-tolerant structure [39]. The IMU has two power supply and processor boards providing internal redundancy. Typically, one processor board and all four gyros are powered at all times, while the four accelerometers are powered only when performing a trajectory correction maneuver (TCM). Spacecraft attitude is estimated by the MP software using a Kalman filter algorithm to combine star tracker and gyro measurements. A simpler filter is used to estimate accumulated velocity change from accelerometer measurements when executing TCMs.

This set of sensors ensures system's constancy: the Sun sensors alone could not perform attitude determination during the eclipse phases, while the IMU suffers from accumulated errors over time. Star sensors provide fine attitude determination, but are expensive in terms of operations on board for data processing. During nominal operations, attitude determination is achieved through one star tracker, and four gyroscopes. Using one star tracker and four gyroscopes can provide redundancy and help improve the overall reliability of the attitude determination system. The star tracker can provide accurate attitude measurements based on star observations, while the gyroscopes can provide continuous rate information. By combining the measurements from both sensors, it is possible to estimate the spacecraft's attitude with higher accuracy and robustness. Additional sensors such as sun sensors and additional star trackers can be used to enhance the accuracy and reliability of the attitude determination system and of course, they are essential in case of failure.

4.1.2 Actuators

The actuator suite consists of reaction wheels and thrusters.

	Name	T_{max} [Nm]	h_{max} [Nms]	Number
Reaction Wheels	Teldix RSI 7-75/601	0.075	7.5	4

Table 4.2: *Reaction Wheels*

The 4 reaction wheels are set in a *pyramid* configuration. This design enables redundancy to the spacecraft to be fully controllable even with the failure of one of the wheels. During nominal operations, attitude control is achieved through the combination of the four reaction wheels.

Thrusters	Thrust Max [N]	I_{sp} [s]	Type	Number
LVA	667	316	Bi-Propellant	1
C	22	230	Monopropellant	4
A,B,S,P	4.4	220	Monopropellant	12

Table 4.3: *Thrusters*

The thrusters are divided into three classes depending on the total amount of force they hand over to the spacecraft. The **LVA** (Large Velocity Adjuster) and the **C**-thrusters provide force in the -Z direction and are devoted to primary propulsion's duties. The **A**, **B**, **S**, and **P** thrusters grant lower thrust levels and are dedicated to secondary propulsion, in order to furnish fine attitude control and momentum management burns; the **A**-thrusters in the +X side and **B**-thrusters in the -X side are disposed in double canted sets of four for redundant attitude control on the three axes, while the **S**-thrusters in the +Y side and the **P**-thrusters in the +Y side entrust velocity changes in the sunward or away-from-the-sun direction respectively.

4.2 Pointing Budget for Control

4.2.1 Control Modes

From a Guidance and Control perspective, flight operations can best be described as the interaction of three spacecraft operational modes with a set of four primary activities. When all systems are performing nominally, the spacecraft is in its “operational” (OP) mode. Demotion to one of two safe modes, safe-hold (SH) or Earth acquisition (EA), occurs autonomously in response to certain faults or by ground command. Promotion from either of the two safing modes to OP mode can occur only via ground command. The four G&C activities are maintaining spacecraft attitude, managing spacecraft momentum, executing TCMs, and pointing the two solar panels.

OP mode is the normal mode for science observations and engineering activities. All varieties of the four primary G&C activities can be performed in this mode. Spacecraft attitude is altered by command as needed to point antennas at the Earth, point instruments at various science targets, or align thrusters with a target ΔV direction. A wide variety of pointing options are available for pointing in inertial directions, to various celestial bodies, and to locations on one of these bodies. Scan patterns combining periods of fixed rate rotations about specified axes with pauses can be added to the base pointing option. One star tracker and four gyroscopes are used during nominal operations, while the other sensors ensure reliability of the measurements and redundancy.

All reaction wheels are used for maintaining attitude, while A,B,S and P thrusters are used for slew maneuvers and RWs desaturation burns. The number and exact thrusters used depend on the quantity and direction of torque needed as well as the spacecraft’s orientation with respect to the sun, as all burns must ensure that the shield stays pointed to the sun at all times during the inner cruise and Mercury orbit phases.

The spacecraft enters SH mode when a fault of intermediate criticality is detected. Commanded execution of TCMs or momentum dumps is prohibited in this mode. Spacecraft attitude is restricted to the ”downlink” attitude, which aligns a specified body axis with the Sun line, in order to satisfy the SKI constraint, and places the Earth line in one of the quadrants of the XY plane covered by one of the two antenna sets, permitting communication with Earth. If the HPKO constraint is enabled, the attitude will be adjusted away from the downlink attitude when necessary to keep the top deck pointed away from the planet’s surface. Once the spacecraft passes out of the defined hot-pole region, normal downlink pointing is automatically reestablished. On entry to SH mode, solar panel control is set to the fixed Sun offset mode using a specially designated value for the size of the offset angle. The offset angle value can be changed or one of the other two control modes (panels in a fixed angle in the body frame or sun offset mode with temperature offset) can be invoked by ground command once in SH mode. Despite SH mode being a non-nominal condition, there are no other severe constraints on the sensors, apart from the ones demanded from attitude’s requirements.

The spacecraft goes into its lowest level safing mode - EA mode - in response to faults of highest severity. As in SH mode, execution of TCMs or momentum dumps is prohibited, and commands to change to one of the other pointing options are ignored. A specific “Sun-relative rotisserie” attitude is automatically implemented. The rotisserie attitude points a specified spacecraft body axis at the Sun and rotates the spacecraft about this axis at a fixed rate. The nominal EA Sun line is either the +Y or -Y axis, depending on spacecraft range from the Sun, and the rotation rate is 0.0005 rad/s, taking 3.5 hours to complete a single revolution.

This rate and the axis can be altered by command. While star tracker data are used if available, the EA attitude can be achieved using only Sun sensor and gyro rate measurements. If both star tracker and Sun sensor data are lost, the system switches to a Sun search routine that performs a series of rotations about each of the body axes until Sun direction information is restored. On entry to EA mode, solar panel control is set to the body-fixed angle mode using a specially designated value for the position angle. The body-fixed angle value can be changed or one of the other two control modes can be invoked by ground command once in EA mode.

In any of the three modes, the G&C system monitors system momentum and will initiate a momentum dump using thrusters when momentum magnitude exceeds limits that could compromise controllability using the wheels [7].

4.2.2 Pointing budget

When in operational mode the pointing budget is dictated by the accuracy requirements of the scientific instruments on board. The pointing precision needs to be at least 0.1° and the pointing knowledge at least 0.02° considering the most requiring instrument [35]. The requirements are satisfied by using star trackers (accuracy ranging from 0.0003° to 0.01° [36]) together with reaction wheels. In the other two control modes, the pointing accuracy is the one needed to point the antennas at Earth and the Sun shade and solar panels at the Sun. The Sun shade axis has to stay within 12° from the Sun line, the antennas have a 12° wide beam and the solar panels don't need a high precision pointing, so using the star trackers and Sun sensors, together with reaction wheels provides enough accuracy [7].

4.3 Disturbances

4.3.1 External Disturbances

Counter acting the disturbances coming from the environment is crucial in order to pursue the scientific objectives of the mission and to perform the attitude control's operations; a preliminary estimation of the predominant torques acting on the spacecraft during its mission is performed. The most relevant phases are the fly-by performed around Earth, Venus, and Mercury. Since for Venus and Mercury multiple fly-bys are performed, the ones taken into account are those with the closest approach to the surface.

	Earth fly-by	Venus fly-by	Mercury fly-by
Gravity gradient [Nm]	$2.10 \cdot 10^{-4}$	$3.85 \cdot 10^{-4}$	$3.43 \cdot 10^{-4}$
Solar radiation pressure [Nm]	$1.50 \cdot 10^{-6}$	$2.88 \cdot 10^{-6}$	$9.87 \cdot 10^{-6}$
Atmospheric drag [Nm]	$\simeq 0$	$\simeq 0$	$\simeq 0$
Magnetic field moment [Nm]	$4.79 \cdot 10^{-4}$	$\simeq 0$	$1.30 \cdot 10^{-5}$

Table 4.4: Worst-case external disturbance torques

Thanks to the results provided by the NASA's missions MESSENGER and MARINER 10, which provided informations about the intensity and the direction of the magnetic field of Mercury, it is has been possible to provide an estimate of the torque related to its presence. Anyway, studying the magnetic field of Mercury is one of the scientific goals of MESSENGER: before the launch, the only data on Mercury's magnetic field were the ones provided by MARINER 10, which covered a very limited part of the planet and computed a low amount of data. Because of that, the torque induced by the external magnetic field has not been taken into account.

4.3.2 Internal Disturbances

A possible internal disturbance all along the mission is propellant mass distribution that could change the position of the center of mass. The way this problem is handled is by emptying both fuel tanks simultaneously so that symmetry is maintained. Fluid sloshing could potentially be a relevant disturbance, but it is minimized by adding baffles inside the propellant tanks. All sorts of misalignments and uncertainties around the center of mass are considered by positioning it a few centimeters away from it's real position. Moreover, structural dynamics due to flexibility of some components (especially the appendages) and thermal shocks, given by the rapidly changing distance from the hot surface of Mercury, have to be considered.

4.4 Reverse Sizing

4.4.1 Subsystem mass sizing

In Table (5.5) are shown the masses for the different components of the ADCS subsystem according to the literature.

—	Quantity	Mass [kg]
Reaction wheels	4	15
Star trackers	2	5
Sun sensors	2	2.6
Inertial measurement unit	1	5.6
Total		28.2

Table 4.5: Mass sizing

The total mass obtained is very similar to the real one of about 27 kg [37].

4.4.2 Reaction wheels sizing

The reaction wheels provide attitude control to the spacecraft by counteracting the external disturbances and performing slew maneuvers. The previous analysis shows that the amount of external disturbances is considerably high when the spacecraft is in proximity of the Earth, however having taken in consideration both the importance of the orbital phase around Mercury for the accomplishment of the scientific goals of the mission and the time duration of this phase, the sizing of the actuators is estimated taking into account the torques the spacecraft undergoes to in Mercury's environment.

Station keeping

The total torque has been estimated taking in consideration the two main disturbances acting on the spacecraft: the solar radiation pressure and the gravity gradient at a given distance R from the main attractor Mercury.

$$T_{GG} = \frac{3\mu_{pl}}{2R^3} (I_{Max} - I_{Min}) \cdot \sin(\theta) \quad \text{Gravity gradient} \quad (4.1)$$

$$T_{SRP} = \frac{F_S}{c} (2A_{pn}(1+q_{pn}) \cos(\alpha) \Delta x_{pn} + A_{ss}(1+q_{ss}) \Delta x_{ss}) \quad \text{Solar Radiation Pressure} \quad (4.2)$$

where the subscript pn refers to the solar panels and the subscript ss refers to the sunshade. Moreover notice that:

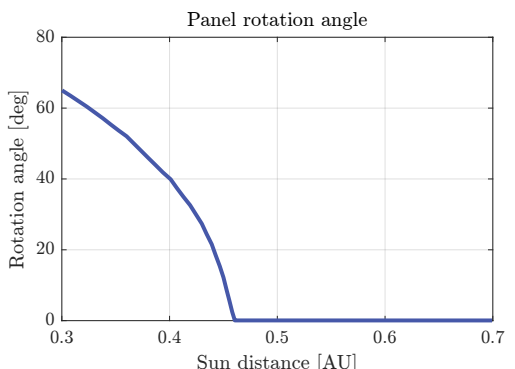
F_S is the solar energy flux density

θ is the orbit-averaged deviation of the z-axis from the local vertical

α is the angle between the solar panel and the sun direction

Δx is the distance between the center of solar pressure and the spacecraft center of mass

q is the reflectivity coefficient of the body



Since the orbit of Mercury periapsis is equal to 0.31 AU and its apoapsis is 0.47 AU the value of α has been considered to be changing accordingly.

By considering an averaged value of the Gravity Gradient along the orbit around Mercury during the first part of the scientific phase (i.e. 12 h, 200×15200 km orbit), it is possible to compute the total angular moment absorbed by the spacecraft leading to the following results.

Single RW storage [Nms]	RW number [-]	Computed CMD [-]	Real CMD [-]
7.5	4	64	41

Table 4.6: Commanded Moment Dump manoeuvres

The number of momentum dumps calculated is higher than the one actually performed by the spacecraft, as MESSENGER's solar panels were cleverly used in order to generate an SRP torque that was capable of reducing the accumulation of momentum in the reaction wheels.

One further detail that was not modeled in our calculation is the fact that the orbit-averaged effect of the gravity gradient torque is much lower than the mere integral of the gravity gradient along one complete orbit: this is due to the fact that some of the momentum stored during half of the orbit can be used to counteract the torque perceived by the spacecraft during the other half of the orbit.

This computation is therefore to be intended as a worst case scenario, where all of the applied torque is counteracted by the reaction wheels.

Slew manoeuvres

Given the fact that MESSENGER mostly held a inertial sun pointing attitude due to thermal constraints, the main slew maneuvers performed were 3 *Flip maneuvers* and 2 *Flop maneuvers* when crossing the 0.95 AU distance from the Sun, to orient respectively the sun shield *towards* and *away from* the Sun.

Considering a slew manoeuvre, with constant acceleration and breaking, the torque needed by the reaction wheels is:

$$T = 4\theta_{max} \frac{I_{max}}{t_m^2} \quad (4.3)$$

where:

- $\theta_{max} = 180$ is the maximum slew angle possibly needed around the major inertia axis;
- $I_{max} = 467 \text{ kgm}^2$ is the major inertia moment;
- $t_m = \frac{\theta_{max}}{\dot{\theta}_{max}}$ is the minimum slew manoeuvre time, considering the acceleration as $\dot{\theta}_{max} = 0.5^\circ/\text{s}$;

The resulting torque needed for this type of maneuver is $T = 0.045N$, which is under the maximum torque which a reaction wheel can provide.

4.4.3 Thruster sizing

Reaction Wheels desaturation can be performed passively by changing the solar panels orientation to exploit the solar radiation pressure or actively by firing a set of eight thrusters (A and B sets). Anyway, due to the frequency of scientific observations during the orbital phase around Mercury the passive dumping is no more sufficient; a sequence of commanded moment dumps (CMD)

is scheduled in order to avoid saturation of the reaction wheels [34].

Firstly, the minimum time required to desaturate is computed:

$$t_{min} = \frac{h_{max}}{n_{th}LF_{max}} \quad (4.4)$$

where:

- $h_{max} = 7.5 \text{ Nms}$ is the maximum angular momentum storable by one wheel;
- $n_{th} = 2$ is the number of thrusters responsible for each one of the four reaction wheels;
- $L = 1.12 \text{ m}$ is the arm of the torque;
- $F_{max} = 4.4 \text{ N}$ is the maximum force which each thruster can provide

This computation results in $t_{min} = 0.76 \text{ s}$, which is compatible with the minimum burning time of the 4.4 N thrusters used for this application. However, the reaction wheels cannot despin fast enough to keep up. The burn is therefore divided into multiple smaller impulses that take place over a time window of roughly one minute[10].

4.4.4 Mass budget

It is possible to compute the propellant mass by combining the duration of each momentum dump manoeuvre and the total number of dumps required according with the following equation:

$$m_p = n_{dumps} \cdot \frac{n_{wh} t_b F_{th}}{I_{sp} g_0} \quad (4.5)$$

where:

- $I_{sp} = 220 \text{ s}$ is the specific impulse of the thrusters;
- $n_{dumps} = 181$ is the total number of momentum dumps;
- $n_{wh} = 4$ is the number of reaction wheels;
- $t_b = t_{min}$ is the burning time;
- $F_{th} = F_{max}$ is the force applied by one thruster.

This results in a propellant mass needed of 1.12 kg .

Assignment 5: TCS subsystem

5.1 Introduction

Perhaps the single most challenging aspect the MESSENGER Mission, was the spacecraft's Thermal Control Subsystem (TCS) design. The probe must in fact be able both to withstand Mercury's harsh thermal environment as well as conciliate this aspect with its survivability along the travel towards the innermost planet.

More in depth:

- Mercury's orbit brings the planet, and the spacecraft, to within 46 million kilometers from the Sun, about 0.3 to 0.47 AU, corresponding to a solar flux variance from 11.1 to 4.5 times stronger than the one of our planet. The flux is unidirectional and is effectively attenuated by the sunshade.
- A secondary problem, that nevertheless cannot be underestimated, is the presence of the hot, broiling surface of the planet itself, 433°C at perihelion and 298°C at aphelion, with a reflected solar intensity of approximately four times that on Earth. In contrast with the Sun's flux this thermal flux is omnidirectional.

5.2 Architecture

The MESSENGER Thermal Control Subsystem (TCS) is designed to work in completely passive way, requiring no louvers or other mechanisms, and requires little heater power, minimizing both weight and power demands. The materials used are readily available and proven low risk.

MESSENGER TCS has three main design elements:

- A ceramic-fabric sunshade
- Multi-layer insulation
- Heat Radiators

5.2.1 Sunshade

MESSENGER's peculiar and most important tool of thermal defense is a heat-resistant and highly reflective sunshade, fixed on a titanium frame to the front of the spacecraft. Measuring about 2.5 m tall and 2 m across, the thin and light, around 20 kg, shade has front and back layers made of 3M Nextel 312-AF 10 ceramic cloth surrounding several inner layers of aluminized Kapton plastic insulation. While temperatures on the front of the shade could reach 325-370° C when Mercury is closest to the Sun, behind the shade the spacecraft will operate at a temperature around 20° C. The ceramic cloth is rated for temperatures in excess of 1000°C. Adequate testing was done on the sunshade, that was soaked, not cleaned, at 355° C for 18 days, around 432 hours [49].

5.2.2 Multilayered insulation

Made with Kapton and other insulating hardware, MLI covers most of the surfaces of the spacecraft to protect it against incident thermal radiation and insulate it against internal heat loss. This second level of thermal protection assumes a key role against heat radiation coming from Mercury's surface.

5.2.3 Radiators

OSRs covered, connected to diode "one-way" heat pipes, radiators are installed on the sides of the spacecraft to carry heat away from the spacecraft body, channeling the heat on the side of the spacecraft that is not in view of the planet. Radiators are isolated from the spacecraft structure and electronics, being coupled only through radiation. A total of 1.2 m^2 of radiator area is needed to dissipate internal heat. They are located on the +X and -X faces of the spacecraft since the -Y face contains the sunshield and +Z and -Z faces contains the LVA and the launch vehicle adapter [48] [43].

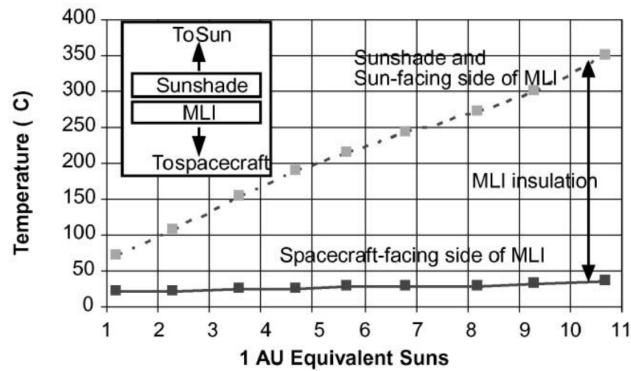
The choice of diode heat pipes is dictated by the fact that when a radiator is facing Mercury's hot side, heat flux would be inverted and this would lead to an increase in temperature of the internal electronics connected to the heat pipes. The unsymmetrical heat transfer coefficient of the diode pipe prevents this from happening, effectively detaching the radiator from the rest of the spacecraft's thermal subsystem. Nominal heat flux is restored once the radiator is back in full view of deep space and has cooled down sufficiently.

5.2.4 Heaters

Other important hardware components in the thermal subsystem design are the 33 redundant heaters, divided in primary and secondary heaters. The set-points of the primary and secondary heaters are offset so that the secondary heaters are never energized unless a primary heater fails. Battery temperature relies on two redundant heater that are controlled by mechanical thermostats.

5.2.5 Structure

The structure of MESSENGER was designed to endure to the extreme heat, featuring a graphite composite construction. The spacecraft is also thermal insulated during burns, the large bipropellant thruster is surrounded by a gold-plated heat shield [40].



(a) Temperatures in the various phases, according to distance from the Sun



(b) A view of the sunshade prior to launch

The only elements of the spacecraft, not effectively protected by the sunshade are the solar panels. For this reason they are placed on low-conductive struts, 0.9 m from the side radiator panels to reduce heat coupling to the spacecraft. The back faces are covered by Kapton with a vapor deposited aluminum outer layer, reducing the expected temperature by 150°C over that of a fully-packed array.

All these solutions, combined together with the addition of a smart mission design, tailored towards heat management strategy, largely removed the thermal burden from the other subsystems, allowing the spacecraft to operate without the use of special high-temperature electronics, as well as traditional components and design[44].

5.3 Phases

This particular mission is strongly constrained under the thermal viewpoint, comprehending extreme as well as disparate environments. Due to these aspects, mission design plays also a key role in the thermal management strategy, both during the cruise phase and the orbiting around Mercury, bringing to a precise formulation of the various phases[47] [8].

5.3.1 Cruise phase

During the outer cruise phase of the mission, the focus is switched towards the necessity to prevent an overcooling of the spacecraft. At the beginning of the mission, after launch with the sunshade pointing towards the Sun, the spacecraft will use heater power to make up for the correct thermal condition that cannot be achieved otherwise.

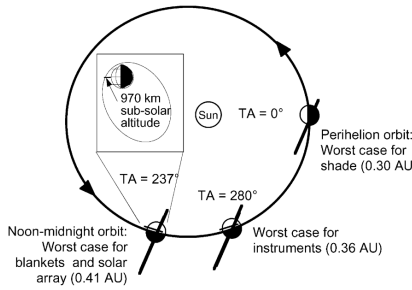
In order to reduce heater power consumption and increase solar array power margin, MESSENGER is designed to be flipped such that the side opposite to the sun shield can be illuminated during outer cruise. This capability has allowed MESSENGER to operate easily between 0.95 and 1.08 AU with little heater power required, allowing unconstrained outer solar distance flexibility when the mission design team was planning for back-up trajectories without complicating the spacecraft thermal or power designs. The spacecraft remained directly exposed to Sun light until 0.95 AU, in the so called outer cruise. To counteract the cooling, a series of “flips” and “flops” were planned. The “flip” maneuvers positioned the sunshade towards the Sun. The “flop” maneuvers turned the spacecraft and pointed the sunshade away from the Sun (see fig:5.2c).

5.3.2 Orbital phase

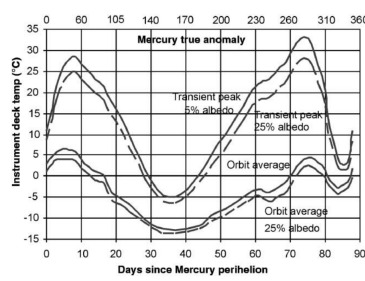
The science orbit has been designed to limit the spacecraft exposure to the heat re-radiating from the surface of Mercury. MESSENGER will only spend approximately 25 minutes of each 12-hour orbit crossing at low altitude, around 200 km, from Mercury's surface, in order to prevent overheating. The maximum surface temperature of Mercury reaches 433°C at the subsolar point and drops off as a cosine function from the maximum to -173°C . The IR heat flux is omnidirectional and cannot be effectively attenuated by the sunshield, thus, in order to minimize this problem, a choice was done in the spacecraft's orbit design: it was designed to be highly elliptical with a periapsis latitude at 60°N . In this way it was possible, in most of the cases, both to place the periapsis of the orbit far from the subsolar point, both to pass the subsolar crossing point with a high velocity. Furthermore, when the orbit periapsis is the nearest to it, Mercury is at 0.41 AU from the Sun or 273° true anomaly: far enough from its perihelion. The spacecraft attitude is controlled to keep the sunshade between the body of the spacecraft and the Sun. This restricts the spacecraft pitch to $\pm 12^{\circ}$ and yaw to -17° through $+13.5^{\circ}$.

The worst thermal case for the instruments occurs when the spacecraft periapsis is near the subsolar point, day 75, at a distance 0.36 AU from the Sun.

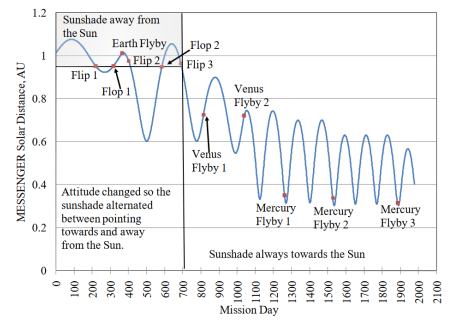
The worst transient, so the broadest variation in temperature experienced by the instruments, is 33°C and lasts for only 25 minutes, with a maximum temperature gradient of 1.5°C per minute. Fortunately this occurs only during a small portion of the orbit. In fact in the remaining part of the 12-hour orbit, the temperature is close to the orbit-average value. [8] Thus the payload is kept within its operating temperature range over 99.5% of the orbit phase, with survival margins in excess of 20°C . Also, spacecraft electronics are always within their -29°C to $+60^{\circ}\text{C}$ operating range, with less than a 5°C per minute gradient. The battery always remains within its -10 to $+25^{\circ}\text{C}$ operating range. For the majority of the mission, the battery temperature is maintained by heaters to be between -5 and 0°C . [8] During the eclipse, the battery temperature does peak to 19°C , but lifetime concerns are mitigated because only 200 discharge cycles are expected.



(a) Where the described conditions occurs along the orbit



(b) Average and peak instrument deck temperatures



(c) Flip Flop manoeuvres

5.4 Reverse Sizing

Reverse sizing of the thermal control subsystem will be performed by analyzing and justifying through numerical models the choices adopted by the engineering team of the MESSENGER mission.

5.4.1 Thermal environment

In the cruise phase, the main source of heat is represented by the radiation coming from the Sun. In the outer cruise ($d_{\text{Sun}} > 0.95\text{ AU}$), the solar flux has been modeled as a function of the distance between the spacecraft, or the planet Mercury as in the following case, and the Sun

$$q_{\text{Solar}}(r_{\text{SC}}) = q_0 \left(\frac{r_{\text{Earth}}}{r_{\text{SC}}} \right)^2 \quad \left[\frac{W}{m^2} \right] \quad (5.1)$$

where q_0 is the solar flux ad 1 AU .

In the inner cruise instead, the solar flux has been decreased by a factor to account the effect of the sunshield blocking a large part of the solar radiation coming from the Sun. The value of the sunshield thermal efficiency η_{SS} , intended as the ratio between the solar radiation that would hit the spacecraft with the sunshield and without it, has been estimated by retrieving the values of absorptivity and emissivity of the outer layer both of the shield and of the spacecraft.

In the Orbital phases, different sources of radiation are present and have been modelled as follows. The albedo heat flux has been modelled as:

$$q_{Albedo} = q_{Solar} \cdot a_M \cdot \cos \theta \cdot \left(\frac{r_M}{r_{SC}} \right)^2 \quad \left[\frac{W}{m^2} \right] \quad (5.2)$$

where a_M is the planetary albedo, known to be 0.08 [50] [51], and θ is the irradiance angle between the spacecraft and the planet.

The IR emission of Mercury's surface is modelled as

$$q_{IR} = \sigma \cdot \epsilon_M \cdot T_{eq}^4 \cdot \left(\frac{r_M}{r_{SC}} \right)^2 \quad \left[\frac{W}{m^2} \right] \quad (5.3)$$

Mercury shows a huge difference in temperature between the subsolar point $\approx 700\ K$ and its dark side $\approx 100\ K$ with high temperature gradient in the illuminated face. Moreover, the orbit periapsis is at 200 km altitude at 60° with respect to the subsolar point [43]. As a consequence, in order to obtain meaningful results in a first approximation, it is necessary to consider Mercury infrared radiation as a black body spectrum ($\epsilon_M = 1$) with equivalent temperature $T_{eq} = 434\ K$ [45].

5.4.2 Spacecraft modeling

In first approximation the spacecraft has been modeled as a single spherical node with total area equal to the main body area $A_{SC} = 2(l_1 \cdot l_2 + l_1 \cdot l_3 + l_2 \cdot l_3)$ and cross section equal to $A_{cross} = \frac{A_{SC}}{4}$. The total thermal power entering and exiting the spacecraft has been computed as:

$$\begin{aligned} Q_{IN} &= Q_{Solar} + Q_{IR}^{IN} + Q_{ALB} + Q_{GEN} && \text{Input power} \\ Q_{OUT} &= Q_{IR}^{OUT} + Q_{RAD} && \text{Exit power} \end{aligned} \quad (5.4)$$

In particular regarding the thermal power entering the spacecraft:

$$Q_{Solar} = \begin{cases} \frac{\sigma (T_{SS,in}^4 - T_{SC}^4)}{\frac{1 - \epsilon_{SS}}{\epsilon_{SS} A_{SS}} + \frac{1 - \epsilon_{SC}}{\epsilon_{SC} A_{Cross}} + \frac{1}{A_{Cross}}} & \text{If the sunshield points towards the Sun} \\ q_{Solar} \cdot \alpha_{SC} A_{Cross} & \text{If the sunshield points opposite the Sun} \end{cases} \quad (5.5)$$

$$Q_{IR}^{IN} = q_{IR} \cdot A_{SC} \cdot \epsilon_{SC} \cdot F_{M \rightarrow SC} \quad (5.6)$$

$$Q_{ALB} = q_{Albedo} \cdot A_{SC} \cdot \alpha_{SC} \cdot K_a \cdot F_{M \rightarrow SC} \quad (5.7)$$

$$F_{M \rightarrow SC} = \frac{1}{2} \cdot \left(1 - \frac{\sqrt{\left(\frac{r_{Orb} - r_M}{r_M} \right)^2 + 2 \cdot \frac{(r_{Orb} - r_M)}{r_M}}}{1 + \frac{r_{Orb} - r_M}{r_M}} \right) \quad (5.8)$$

Notice that in Eq. 5.8, r_{Orb} refers to the orbit radius with respect to the planet while, r_M , refers to the radius of the planet Mercury. Q_{GEN} represents the internal power generated by the spacecraft itself. $T_{SS,in}$ and ϵ_{SS} are taken as the temperature and the emissivity of the sunshield side facing the spacecraft during orbital operations. The power exiting the spacecraft can instead be divided in two contributions: the power irradiated by the spacecraft towards the free space:

$$Q_{IR}^{OUT} = \sigma \cdot \epsilon_{SC} \cdot (A_{SC} - A_{RAD}) \cdot (T_{SC}^4 - T_\infty^4) \quad (5.9)$$

and the power irradiated specifically by the radiators:

$$Q_{RAD} = \sigma \cdot \epsilon_{RAD} \cdot A_{RAD} \cdot (T_{SC}^4 - T_\infty^4) \quad (5.10)$$

According to the literature [46][41][45], the previous parameters have been estimated as follows:

Parameter	Value	Parameter	Value	Parameter	Value	Parameter	Value
ϵ_{SC}	0.05	$A_{SC}\ [m^2]$	13.56	α_{SC}	0.12	$l_1\ [m]$	1.27
ϵ_{SS}	0.87	$A_{SS}\ [m^2]$	5.00	K_a	0.8	$l_2\ [m]$	1.85
ϵ_{RAD}	0.88	$A_{RAD}\ [m^2]$	1.20	$T_\infty\ [K]$	3	$l_3\ [m]$	1.42

Table 5.1: Constants values used

5.4.3 Allowable temperature range

According to literature regarding the mission, all the instruments onboard the spacecraft were designed to operate near room temperature. Taking the highest minimum and the lowest maximum temperature allowed by components, it is possible to determine a safe range of operating temperature for the spacecraft of $0^{\circ}\text{C} < T_{SC} < 30^{\circ}\text{C}$. In this temperature range all of the components are within their temperature limits, even though most of them can also operate well outside this envelope [42]. This will over-constrain the analysis, but will result in a preliminary sizing for the system. A more refined multi-nodal analysis is necessary for this kind of thermal sizing. Normally, a conservative margin of $\pm 15^{\circ}\text{C}$ should be taken over the typical temperature ranges admissible by the various components, but in this case it was possible to retrieve the $0^{\circ}\text{C} - 30^{\circ}\text{C}$ was retrieved from literature [49] as the range used for validation of the thermal model.

5.4.4 Critical cases

Three critical cases have been taken into account to verify properly the TCS subsystem sizing.

Orbital hot case

The first critical case considers the spacecraft in the hottest point of its both interplanetary and planetary trajectory that is the periapsis of the orbit around Mercury.

In this condition the orbital altitude is 200 km and the corresponding view factor between the planet and the spacecraft $F_{M \rightarrow SC}$ is equal to 0.309, while θ is taken 60° in the worst case scenario based on trajectory choice, in the described case the the distance of the spacecraft from the Sun is 0.36 AU, as already described in the Orbital Phase (paragraph 3.2) [8]. In this case, the total thermal power exchanged by the spacecraft, divided in its components is:

Inward				Outward
$Q_{Solar} [\text{W}]$	$Q_{IR}^{IN} [\text{W}]$	$Q_{ALB} [\text{W}]$	$Q_{GEN}^{max} [\text{W}]$	Q_{IR}^{OUT}
69.08	360.11	199.40	450.00	324.68

Table 5.2: Heat fluxes without considering the radiators

The required radiator area to keep the spacecraft at 30°C is 2.06 m^2 while the spacecraft is known to use only 1.20 m^2 of radiative surfaces that, according with this model, will drive the object to a temperature of 58°C . This can be accepted since the model implemented is very simple and the maximum temperature aforementioned is referred only to actual components that are insulated from the structure resulting in overestimating the radiative power required to cool down correctly the spacecraft [44].

The use of diode heat pipes and thermal bridging between heat-producing components and the radiators makes it possible to reduce the need for radiator area to a more manageable size, while allowing for the use of relatively common thermal blanketing materials, such as a multi layer insulation covering the body of the spacecraft, composed of several thin layers of aluminized kapton, which is often used in situations where a cold insulator is required.

It is also possible to estimate the thermal efficiency of the sunshade η_{SS} . According to the previous model, the solar radiation would be 5.9 kW , resulting in efficiency $\eta_{SS} = 0.97$.

Orbital cold case

The second critical case considers the spacecraft in the coldest position of its orbit around Mercury that is the apoapsis in eclipse condition.

The apoapsis is at 15200 km altitude and it would be over the dark side of the planet. In this condition the entering heat flux will involve only the internally generated heat and Mercury's irradiated power while the exit flux will involve the spontaneous radiation towards the free space but also the component due to the presence of the radiators.

For this case $F_{M \rightarrow SC}$ is taken as 0.048 In this situation the heat fluxes involving the spacecraft, which is considered in the lowest accepted temperature, are the following:

Inward			Outward	
Q_{IR}^{IN} [W]	Q_{GEN}^{min} [W]	$Q_{Heaters}$ [W]	Q_{IR}^{OUT} [W]	Q_{RAD} [W]
0.31	220.00	308.09	214.01	314.39

Table 5.3: Heat fluxes in the orbital cold case

$Q_{Heaters}$ was derived as the difference between the outward and inward heat fluxes, computed through the previously shown formulas.

$$Q_{Heaters} = Q_{IR}^{OUT} + Q_{RAD} - Q_{IR}^{IN} - Q_{GEN}^{min} \quad (5.11)$$

In this case the single-node model of the spacecraft is fixed at a temperature equal to $0^{\circ}C$: the lowest admissible one. This results in the minimum power needed to keep the node at the prescribed temperature in steady-state conditions.

The resulting $Q_{Heaters}$ needed is much higher than the one actually required by the mission profile. This is mainly due to the fact that we are considering a steady state condition at the coldest point possible for the mission, while in reality the eclipse phase lasts in the worst case scenario, 35 min, during which steady state condition is not actually achieved[44].

The thermal design of the MESSENGER spacecraft is such that temperature transients take hours to complete, and as such heating power can be limited and directed only to the specific components that need it the most. These include the batteries, fuel tanks, valves, pipings, critical electronic components and processors. The low coefficients of heat transfer of both the MLI and composite structure made it possible to decrease significantly the power requirement during these relatively brief phases.

Interplanetary cold case

The third critical case considers instead the coldest condition encountered during the outer cruise, which happens at a solar distance of $0.95 AU$, when the spacecraft is flipped into the configuration where the sunshade is pointed sunwards. In this condition solar heat flux is only slightly higher than the minimum for the mission, which happens at a distance of $1.08 AU$, but the added effect of the sunshield makes the actual heat flux hitting the spacecraft much lower. Accounting also for the presence of the Sun shade, the expression for the entering heat flux results in :

$$Q_{Solar}^{IN} = (1 - \eta_{SS}) q_{Solar} \cdot \alpha_{SC} \cdot A_{cross} \quad (5.12)$$

Inward			Outward	
Q_{Solar}^{IN} [W]	Q_{GEN}^{min} [W]	$Q_{Heaters}$ [W]	Q_{IR}^{OUT} [W]	Q_{RAD} [W]
18.48	220.00	289.92	214.01	314.39

Table 5.4: Heat fluxes in the interplanetary cold case

As can be seen, the required $Q_{Heaters}$ to keep the spacecraft at the lowest acceptable temperature is lower than in the previous case resulting in a non-sizing condition. This is close to the required increase in power output that happened right after a *Flip* maneuver, which was in the order of $250 W$ [44]. Notice that, as in the Orbital cold case, $Q_{Heaters}$ is computed by taking the difference between the known inward and outward heat fluxes, in particular:

$$Q_{Heaters} = Q_{IR}^{OUT} + Q_{RAD} - Q_{Solar}^{IN} - Q_{GEN}^{min} \quad (5.13)$$

5.4.5 Mass estimation

The bulk of the mass of the thermal control subsystem comes from the radiator panel, which have an honeycomb aluminum structure with an average density around $\rho_{Rad} = 12 kg/m^2$ for space applications. Heaters are typically made up of a thin resistive element protected between two layers of a protective plastic material and do not carry significant weight. MLI mass strongly depends on the number of layers and on the material used, as well as on the design of the supporting structure. A preliminary estimate based on values retrieved from other application returns an average density of $\rho_{MLI} = 1.2 kg/m^2$. An extra margin is considered to account for the mass of the structure holding the sunshield and the body MLI and connecting it to the main structure .

Component	Radiators	Body MLI	Shield MLI	Margin 30%	Total
Mass [Kg]	14.40	14.83	6.0	10.57	45.80

Table 5.5: Mass estimations

The total computed mass is lower than the one retrieved from literature of 52.2 kg [42], which is likely due to the fact that this model does not take into account the weight of heat pipes, heaters, and thermostats due to lack of sufficient documentation regarding size and weight, as well as underestimating slightly the mass of the structure holding the sunshield, which also has to support some antennas, thrusters and sensors during the liftoff phase.

This represents however a good initial approximation of the mass of the subsystem.

5.4.6 Material choice

Reversing the previous equations in order to retrieve the values of α and ϵ of the materials used in the thermal insulation of the spacecraft is not trivial, as with the current simplified model no proven material can satisfy the requests of the mission.

The material with the closest characteristics, however, is aluminized kapton [41], which has a long history in the space industry as a cold coating. This is due to the fact that the hot case of the mission is the most critical one, while heater power can easily be provided during cold cases thanks to the availability of solar power and battery power during the course of the mission.

Assignment 6: EPS subsystem

6.1 EPS components

The MESSENGER power system consists of the Power System Electronics (PSE), the Power Distribution Unit (PDU), the Solar Array Junction Box, the battery, the two solar array (S/A) panels, and the Solar Array Drive Assembly (SADA) 6.1. The nominal bus voltage is 28 V and can vary between 22 and 35 V depending on the state of charge of the battery.

The mission design called for an interplanetary phase that did not require any excursion beyond 1.08 AU with relatively short eclipses, making solar panels and battery a much easier and simpler choice compared to the use of an RTG. Open bus design was also dictated by ample power availability and to reduce subsystem complexity.

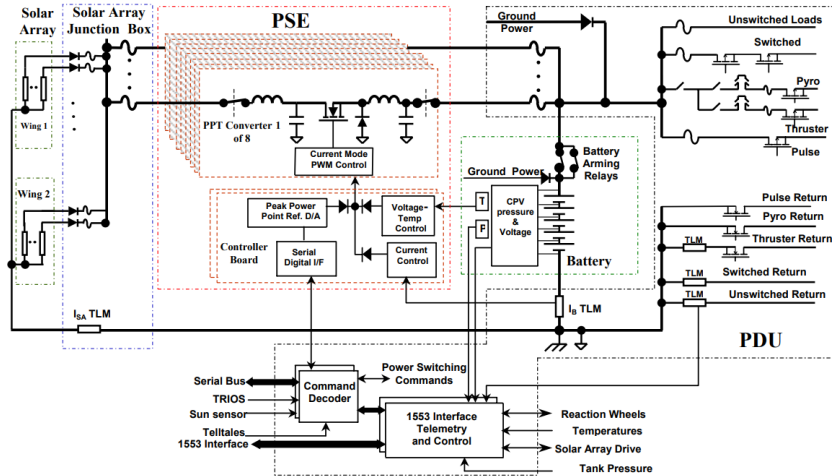


Figure 6.1: Simplified Block Diagram of the MESSENGER Spacecraft Power System

6.1.1 Solar Array

The MESSENGER solar array consists of two deployed single-panel wings. Each panel is 1.54 m wide and 1.75 m long and contains 18 strings of 36 cells each. The strings were placed between Optical Solar Reflector (OSR) mirrors with a cell to OSR ratio of 1:2 to reduce the panel absorbance. The panels are located on the +X and -X faces of the spacecraft, and they stick out of the sunshade and can pivot around the X axis independently from each other.

The panel substrates are 18-mm thick aluminum honeycomb with RS-3/K13C2U composite face sheets. The face-sheets are 0.6-mm thick with local 0.5-mm doublers. The graphite-cyanate-ester materials on the panel face sheets were chosen for their high thermal conductivity, but their mechanical strength is relatively low. Doublers and triplers are therefore required in areas of high stress due to the large panel cantilever in the stowed configuration. The panel front cell side is insulated with 0.05-mm Kapton, co-cured with the graphite fiber face sheet. The back face sheet is covered with co-cured square-shaped aluminized Kapton 30.5 cm x 30.5 cm sheets. The aluminized Kapton is used to lower the absorbance of the backside of the solar panel to a level comparable to the solar cell-OSR side. This ensures that the panel can survive solar illumination with normal incidence to either side at the closest approach to the Sun, even in case of loss-of-pointing of the spacecraft.

The solar cells are 0.14-mm thick, 3 cm by 4 cm triple junction gallium-arsenide cells, with minimum efficiency of 28%. The cells use a standard one-Sun cell top metallization grid design. The cover glass on each cell is 0.15-mm-thick cerium-doped microsheet. The cell interconnects utilize silver plated Kovar material. The wires that carry power and temperature signals are routed along the titanium boom to connectors at the SADAs. Both the wires and the boom are wrapped with multi-layer insulation. The solar panel temperatures are sensed using platinum wire sensors, placed beneath the solar-cell-side face sheet in small bored cavities. To minimize the magnetic field induced by the currents in the strings, adjacent strings are placed with alternating current polarity, and the strings are back wired such that each string return runs under its cells.

6.1.2 Battery

The MESSENGER spacecraft battery consists of 11 two-cell 23 Ah Nickel Hydrogen CPVs (Common Pressure Vessel) housed in a three-piece clam-shell-type mechanical design that meets all thermal-gradient requirements imposed by the mission profile. It was designed and built at APL. The cells are capable of supporting the required 8-year mission life, as well as enable for a mission extension. Bypass switches were placed across each CPV to eliminate the potential of a spacecraft single-point failure caused by an open circuit of a pressure vessel. In the event of a cell open-circuit failure, small diodes provide a current path to blow a fusing element in the activating coil of the bypass switch. This circuit provides protection against an open-cell fault for both charge and discharge operation.

The battery chassis is electrically insulated from the spacecraft structure and connected to the S/C ground through two parallel 20-k Ω resistors. The battery cells were demagnetized, and the inter-cell wiring is designed to minimize the induced magnetic fields. Approximately 300 eclipses are expected during the first year in Mercury orbit, with the maximum eclipse duration during the mission being around 60 minutes. Power is managed during Mercury eclipses to allow adequate reserve battery energy to recover from any attitude anomaly. The maximum Depth-of-Discharge (DoD) expected during Mercury orbital operations is approximately 55%. The battery DoD from launch to Sun acquisition was 18%. The battery is also rated for a maximum discharge current of 14.5 A, and charging current was limited to a trickle charge of ~ 0.15 A during the final 5% of charge to decrease battery degradation.

The battery is located on the -Y face of the spacecraft, closest to the sunshield, to keep the sensitive battery in a location where it could operate for the whole mission in a range of $-10^\circ\text{C} < T_{\text{Battery}} < 0^\circ\text{C}$, with only minor excursions above this range.

6.1.3 Power System Electronics

The PSE contains eight buck-type peak-power-tracking converter modules, each designed to process around 100 W of output power. Each card can dissipate about 8 W. The control loop of the buck converters varies the duty cycle to maintain the input voltage from the solar array wings to the reference value set by the spacecraft command and data handling (C&DH) processor. The peak power tracking converters process all the power from the solar array. The maximum power the PPT trackers can process is around 800 W. The primary and backup controller circuits of the PPT converters and the housekeeping DC/DC converter are on two printed circuit (PC) cards. The maximum PSE power dissipation is 65 W.

The PSE is packaged in slices with one card per slice. There are eight PPT converter slices and two controller board slices. The slices are machined aluminum 6061-T6, in a tongue-and-groove design with venting through joints.

A heat spreader with thermal vias distributes heat dissipations among the slices and provides thermal interface from chassis to heat pipes that are located underneath the spacecraft deck. It is made of machined aluminum 6061-T6, 0.32 cm thick. There are sixteen thermal vias that are 1.9 cm in diameter and 2.86 cm long.

6.1.4 Solar Array Junction Box

The Solar Array Junction Box contains the isolation diodes in series with each string of the two solar array panels, the current shunt resistor of each wing, the peak power tracker module solar array side fuses, and solar array voltage telemetry buffer resistors. The maximum dissipation in the solar array diodes under worst-case conditions is 26 W.

The fuses placed in series with each string inside the solar array junction box protect the input and output fuses of the peak power tracker modules, in case of a short in one of the string isolation diodes, during the fault condition when the battery voltage is higher than the solar array voltage. This condition can occur during a spacecraft attitude anomaly when the spacecraft is closest to the Sun and the solar panels are pointed normal to the sun.

6.1.5 Power Distribution Unit

The Power Distribution Unit contains the circuitry for the spacecraft pyrotechnic firing control, power distribution switching, load current and voltage monitoring, fuses, external relay switching, reaction wheel relay selects, power system relays, Inertial Measurement Unit (IMU) reconfiguration relays, Integrated Electronics Module (IEM) select relays, solar array drives, propulsion thruster firing control, and propulsion latch valve control. There are two independent sides to the PDU: A and B. Onboard telemetry is also collected by the PDU. Each side of the PDU can command all of the PDU's circuitry.

6.1.6 Solar Array Drive Assembly

Each solar panel is independently rotated with a stepper motor actuator with harmonic drive gearing. A cable wrap that allows rotation from -20 to 200° around the X-axis, with zero being the panel normal in the -Y (sunshade) direction, is used to transfer the solar array power and panel temperature signals to the power system electronics. Initially both panels were moved symmetrically to maintain an equal surface temperature, however scientists figured out a way to orient the panels asymmetrically to generate a sufficient SRP torque to reduce the needed number of momentum dumps needed over the course of the mission. This choice allowed for fuel savings that were proven useful during the extended missions [55].

The closer to the sun the mission got, the slimmer the window of allowable operating angles became, as both thermal and power generation limits got to each other as shown in figure 6.2. This made the SADAs a key element to manage during operations near the Sun and in Mercury orbit.

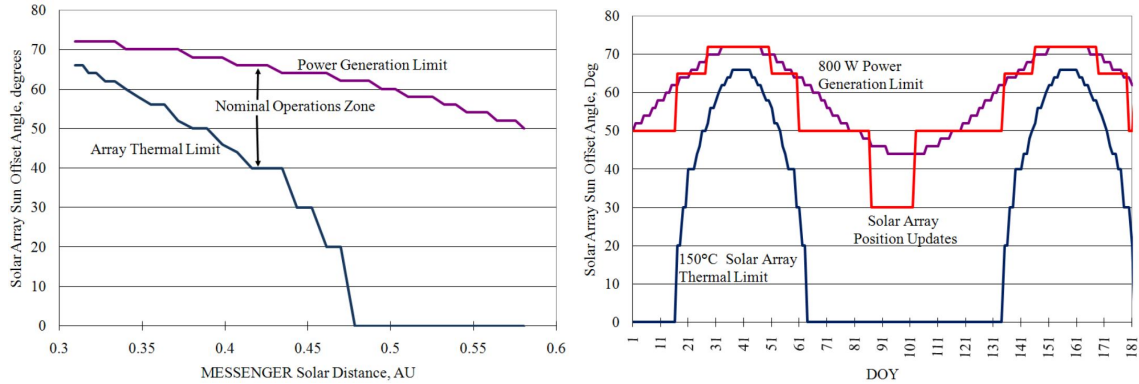


Figure 6.2: Example of limit curves and panel position

6.2 Architecture

6.2.1 Electrical power per phase

Throughout its journey to Mercury, MESSENGER reaches a distance of roughly 0.3 AU from the Sun: this implies strong variation of the intensity of the solar radiation during the mission. Furthermore, during science operations, the spacecraft operates in highly eccentric orbits, with eclipse periods which can sensibly change, meaning not only in discrepancies in the solar power input but also in the requirement of energy supply coming from the batteries. In Tab 6.1 and are displayed the spacecraft's power budget by subsystem [56] :

	Outer cruise (>0.95 AU)	Inner cruise (<0.95 AU)	Orbit ¹	Eclipse phase <th>Eclipse phase<br (<35="" min)<="" th=""/></th>	Eclipse phase
Instruments and heaters	13.2	15.4	95.1	42.6	58.9
IEM	32.7	34.2	33.5	30.2	30.2
Power system	25.6	25.6	105.6	20.9	20.9
TTMC	65.5	65.5	110.5	22.8	25.4
G&C	70.3	70.3	119.7	119.7	119.7
Thermal	10.2	62.2	58.4	10.0	23.8
Propulsion	21.9	95.6	74.6	34.0	47.8
Harness	3.7	7.6	12.0	4.4	5.5
TOTAL	247.8	382.7	597.4	284.6	332.2
Power input from solar arrays	490.0	528.2	720.0	-	-
Maximum DOD	-	-	-	55	36

Table 6.1: Worst case scenario power budget for different subsystems [W]

The main difference between the phase of outer and inner cruise stands in the body's orientation, as if the spacecraft is far enough from the Sun, the sunshade points in the opposite direction in order to reduce

¹Non-eclipsed time window

the heating power required; once the sunshield is flipped back towards the Sun during the inner cruise and Mercury orbit, power consumption jumps up due to the need for more heating required by delicate components such as the tanks, valves, plumbing and delicate electrical components to maintain an adequate temperature.

During the orbit phase pointing requirements become more stringent to allow for the correct pointing of the various scientific instruments, and the instruments themselves are activated and brought into full operation. Telecommunications also ramp up during this phase in order to transmit the collected data back to Earth.

6.2.2 Eclipse management

An important aspect of the mission was power management during eclipse periods. Two main types of eclipses occurred during the mission, each with its set of challenges: the first one, during $< 35\text{ min}$ eclipses is linked to the 14.5 A maximum discharge current, while the other is due to the maximum allowed DOD of 60% during $> 35\text{ min}$ eclipses.

This second condition is the limiting one of the battery sizing, as some eclipses last up to one hour.

Example of short eclipse: Mercury eclipse

During an average Mercury eclipses, lasting about $15 - 20\text{ min}$, battery discharge is not a problem in and of itself, however minor power-downs were still programmed in order to reduce the discharge current of the battery to below the maximum allowed value: this mainly involved spacecraft heaters and non-critical components, allowing scientific data collection to continue unaffected by the eclipse. This lowers the current draw of the spacecraft from the nominal $15 - 16\text{ A}$ to below the 14.5 A limit.

Example of long eclipse: Venus FB1

The first Venus flyby was challenging because the associated eclipse was 56 minutes long, so battery depth of discharge was the primary concern. For this eclipse, a major power-down was designed to keep the battery state-of-charge above 48%. It included the instruments, communications equipment, star trackers, and spacecraft heaters. The power-down and recovery were written into three on-board autonomy protection rules, one for eclipse entry. The first powered off the spacecraft loads at eclipse entry; the second powered on select loads at eclipse exit; the third powered on the remaining loads once the battery reached full charge.

6.2.3 Power regulation

The large variations in the solar distance and in the duration of the eclipses implies a large variation in the solar array maximum power point voltage: for this reason, the power system uses a Peak Power Tracker (PPT) topology which isolates the battery and the bus from the voltage and current large fluctuations, maximizing the solar array power [57].

6.3 Reverse Sizing

6.3.1 Primary source selection and sizing

For the purpose of the mission the selected primary source are solar panels, considering that the spacecraft will always be less than 1 AU of distance from the Sun. The cells chosen are triple junction gallium-arsenide cells, given their relatively high efficiency, radiation resistance and low risk.

In order to size the panels some data are shown in table (6.2):

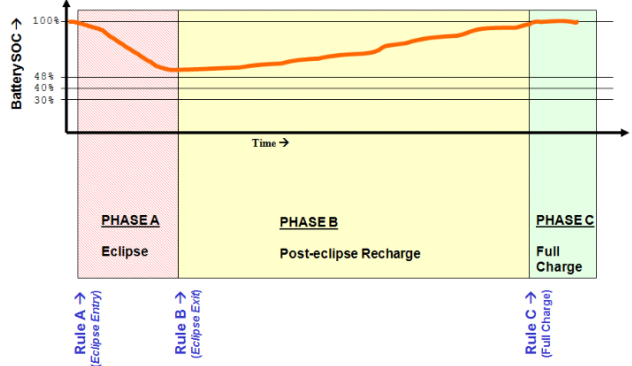


Figure 6.3: Expected battery state of charge during eclipse [55]

Efficiency at beginning of life [-]	$\epsilon_{BOL} = 0.28$	Degradation per year [-]	$dpy = 0.0375$
Inherent Degradation [-]	$I_d = 0.77$	Line efficiency in daylight [-]	$X_d = 0.8$
Line efficiency in eclipse [-]	$X_e = 0.6$	Power request in daylight [W]	$P_d = 597.4$
Power request in eclipse [W]	$P_e = 284.6$	Spacecraft time in daylight [h]	$T_d = 11$
Spacecraft time in eclipse [h]	$T_e = 1$	Mission duration [y]	$T_{life} = 10.75$
Sun irradiance [W/m²]	$I_0 = 9116.4$	Sun-panel inclination angle [°]	$\theta = 65$

Table 6.2: Solar Array Data [54] [56]

The sizing takes into account the most power demanding scenario, which is verified to be during the orbit phase around Mercury, when the array has to satisfy the high power demand, while also recharging the battery.

The first step is to calculate the total power requested by the solar array as:

$$P_{SA} = s \left(\frac{P_e T_e}{X_e T_d} + \frac{P_d}{X_d} \right) = 947.85 \text{ W} \quad (6.1)$$

Where s is equal to 1.2 and represents the ESA system level power margin of 20% [58]. Then the specific power at the beginning of life is found:

$$P_{BOL} = \epsilon_{BOL} \cdot I_0 \cdot I_d \cdot \cos(\theta) = 830.65 \text{ W/m}^2 \quad (6.2)$$

The value of the critical Sun-panel inclination angle θ , which is the maximum one during the course of the mission, is very high due to the necessity to rotate the solar panels every time they reach a temperature of 150°, to dissipate the heat.

The specific power at the end of life can be obtained as:

$$P_{EOL} = P_{BOL} \cdot L_{life} = 550.78 \text{ W/m}^2 \quad L_{life} = (1 - dpy)^{T_{life}} = 0.66 \quad (6.3)$$

Knowing the SA power request and the specific power output at EOL, the SA cells surface and the total surface of the panels (which takes into account the OSRs through a multiplier 3 in the calculation for the total array area due to the ratio of 2:1 OSR to solar cells), can be computed as:

$$A_{cells} = \frac{P_{SA}}{P_{EOL}} = 1.72 \text{ m}^2 \quad A_{SA} = 3A_{cells} = 5.16 \text{ m}^2 \quad (6.4)$$

Finally, knowing that each cell is 3 by 4 cm, the number of cells is found:

$$N = \text{ceil} \left(\frac{A_{cells}}{A_{cell}} \right) = 1434 \quad (6.5)$$

The Solar Arrays are made of different layers of materials : Honeycomb Aluminium for the biggest part but also Kapton used for the OSR mirrors and different carbon fibers positioned at different ply angles to improve the mechanical properties [53]. Here densities and thicknesses retrieved from literature have been summarized:

	Density [kg/m³]	Thickness [mm]
Honeycomb Aluminium Alloy 5056	72	14
K13C2U/RS-3 Carbon Fiber	1750	1.152
K13C1U/RS-3 Carbon Fiber (Doublers)	1750	2.032
RS-4A	1210	0.510
Kapton	1420	0.102

Table 6.3: Solar array layers and thickness

A possible value for the density of the Solar Arrays can be deduced: $\rho_{SA} = 412.56 \text{ kg/m}^3$ taking into account the proportions of each material to the total thickness. The total thickness for the Solar Arrays is $t = 1.8 \text{ cm}$. The mass of the solar arrays can be computed as: $m = \rho_{SA} \cdot A_{SA} \cdot t$.

	A_{SA} [m ²]	N_{Cells} [-]	m_{SA} [kg]
Reverse sizing	5.16	1434	37.90
Real	5.39	1368	34.12

Table 6.4: Sizing results and comparison

The calculated size of the solar array takes into account both solar cells and OSRs areas with perfect packing efficiency, while the area of the real solar array is retrieved from literature and includes gaps between adjacent elements. The value of the effective area of solar cells and OSRs in the real case is 4.92 m², that is coherent with the lower number of cells with respect to the computed one.

The mass discrepancy is likely due to the fact that no information was found on the specific locations where the doubler layer of composite was used. The computation supposes the layer is used everywhere on the panel and results in a preliminary result, which is not too dissimilar from the real result.

The cell number and panel area is linked to the fact that MESSENGER's solar array was designed to accommodate the loss of a line of cells, while still providing enough power for the orbital phase of the mission.

6.3.2 Secondary source selection and sizing

During the analyzed mission the spacecraft has passed through many solar eclipse phases, therefore a secondary power source was needed. The selected source is a Ni-H₂ battery, well suited for long lasting missions, as Lithium ion batteries were still not mature enough and too expensive at the time of launch.

Technology	Energy density (Wh/l)	Specific Energy (Wh/kg)	Specific power (W/Kg) (short pulse)	Cycle number (100% DOD)	Optimum operating temperature range (°C)	Energy efficiency	Self discharge	Comments
Ni-Cd	90	30	200	2000	0 to 40	70-75%	Moderate	
Ni-H ₂	50	55	150	2500	-10 to 30	70-75%	High	
Li-ion	250	150	2000	3000	10 to 40	>95 %	Low	Low Thermal dissipation
Advanced Li	>300	>200	>2000	>2000	-10 to 40	>95 %	Low	

Figure 6.4: Possible secondary battery choices

In order to size the battery some data are shown in table, retrieved from literature and from an analysis of the orbit (6.5):

Spacecraft time in eclipse [h]	Power request in eclipse [W]	Specific energy [Wh/kg]	Energy density [Wh/dm ³]
$T_e = 1$	$P_e = 284.6$	$E_m = 60$	$E_v = 50$

Line efficiency [-]	Cell voltage [V]	Battery capacity [Ah]	Bus voltage [V]
$\eta = 0.85$	$V_{cell} = 1.55$	$C_{cell} = 23$	$V_{bus} = 28$

Table 6.5: Battery data [56] [54]

The battery capacity required to fulfill the power demand is calculated as:

$$C_r = \frac{T_e P_e}{(DoD) N \eta} = 608.77 \text{ Wh} \quad (6.6)$$

where $N = 1$ is the number of batteries and $DoD = 55\%$ is the maximum depth of discharge. This value, for the expected number of eclipses (around 300), falls well within the working range of a Ni-H₂ battery. The number of cells in series is then obtained as:

$$N_{cells} = ceil\left(\frac{V_{bus}}{V_{cell}}\right) = 19 \quad (6.7)$$

This value needs to be increased from the resulting 19 to 22, in order to add the possibility to bypass one CPV (containing 2 cells) in case of failure. Then it is possible to retrieve a new value for the bus voltage

and finally the total string capacity.

$$V_{bus,new} = N_{cells} V_{cell} = 34.10 \text{ V} \quad C_{string} = \mu C_{cell} V_{bus,new} = 627.44 \text{ Wh} \quad (6.8)$$

Where $\mu = 0.8$ is a typical value of the package efficiency. The string capacity is already higher than the required capacity, which means that only one string is needed. Mass and volume of the battery can be found as:

$$m_{batt} = \frac{C_{batt}}{E_m} \quad V_{batt} = \frac{C_{batt}}{E_v} \quad (6.9)$$

where : $C_{batt} = C_{string}$ because there is only one string needed.

The sizing results and a comparison with the real values are shown in table (6.6).

	C_r[Wh]	N_{Cells}[−]	C_{batt}[Wh]	m_{batt}[kg]	V_{batt}[dm³]
Reverse sizing	608.77	22	627.44	10.46	12.55
Real	N/A	22	655.50 ²	24.50	41.09

Table 6.6: Sizing results and comparison

The capacity of the real battery is computed as : $C_{batt-real} = 23 \text{ Ah} \cdot V_{batt}^{Avg}$. The mass and volume values are much lower than the real ones, because they don't include the 11 common pressure vessels and the rest of the structure.

²Supposing 23 Ah at an average of 28.5 V

Assignment 7: CONF and OBDH sub-systems

7.1 Configuration

7.1.1 Space Segment

The MESSENGER mission was launched on 3 August 2004 on a Delta II launch vehicle from Cape Canaveral. The size of the spacecraft is dictated by the need to keep the mass low enough to be inserted into a energetic enough orbit, while the dimensions are limited by the fairing size [59].

The very first configuration that is considered is the "folded" configuration. The spacecraft is folded to fit inside the launcher's fairing and will need to withstand the harshest mechanical environment during launch. The mechanical environment can be described across several loads that must be considered for a preliminary design:

- Static and dynamic loads
- Stage separation
- Payload fairing separation
- Random vibrations
- Acoustic loads
- Shocks

The spacecraft is protected from atmospheric heating and loads by the fairing which also has some constraints over the payload. In fact, the whole structure of the "folded" payload shall be contained within the fairing dynamic envelope which protects the spacecraft from launch vibrations with sufficient margin.

In figure 7.1 is displayed the folded spacecraft, during the integration with the fairing. Below it the third stage kick motor is visible. The spacecraft is attached to the rocket by an attach fitting, located at the center of the -Z face (see figure 7.3), which transfers the aforementioned loads between the two. Numerical accurate simulations and vibration tests were done to ensure the spacecraft's safety along the launch.

The only difference between the folded and unfolded configuration can be found in the solar arrays and the extending boom for the magnetometer, which are retracted to fit inside the allotted space inside the fairing of the Delta-II: the two solar arrays are folded against the body of the spacecraft through a single hinge for each panel, with a positive stop to prevent them from touching the spacecraft's body, while the 3.6 m arm is stowed through two hinges (see figure 7.2). Deployment of the solar arrays and the magnetometer boom happens soon after the injection in the escape trajectory to allow for testing and validation of the components.



Figure 7.1: "folded" configuration during integration in the fairing



Figure 7.2: Folded configuration

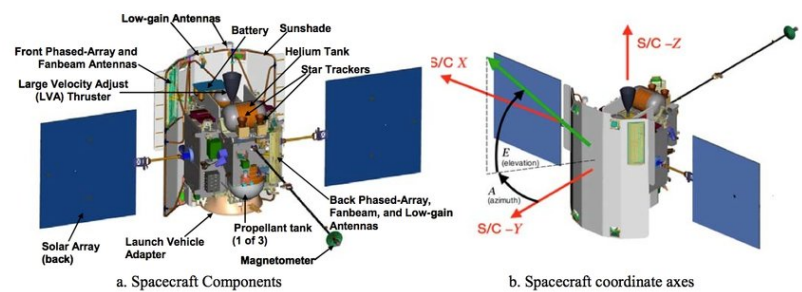


Figure 7.3: Unfolded configuration

The following sections are based on literature ([61], [63], [64]) and a critical analysis of the spacecraft configuration.

Thermal subsystem

The first design choice was the orientation of the Sunshade towards the sun along the flight to withstand the extreme temperatures. Therefore, the choice of positioning it in the -Y face was the driver for the system configuration.

The two main radiators are mounted flush on the +X and -X faces, the largest available ones, of the body in a symmetric way to avoid center of mass (CoM) imbalance. This position allows them to have a clear view at empty space, without ever being pointed to the sun.

Power subsystem

The Solar Arrays are in the classic symmetrical configuration to assure symmetry in weight distribution and SRP torque effect. The faces selected for the design are +X/-X, with poles that extend the panels outside the shade of the sunshield.

The battery is located on the -Y face of the spacecraft, closest to the sunshield, to keep it in a location where it could operate for the whole mission in a range between -10°C and 0°C , with only minor excursions above this range. This position has the advantage of being shielded from Mercury's albedo and IR emissions by the spacecraft body for most of the orbits.

The power system electronics (PSE) and power distribution unit (PDU), solar array junction box (SAJB) as well as the two solar array drive assemblies (SADAs), are located near the base of the poles of the solar panels in order to minimize wiring and in a way that balances out the mass distribution; this also allows the heat generated by the high power electronic components to be easily transferred to the radiators, located nearby.

Propulsion subsystem

In order to avoid ejecting exhaust gasses into the sunshade, the solar panels or the scientific instruments, the only direction to place the powerful 667 N LVA thruster and the four 22 N thrusters is along the Z axis. The choice fell onto the -Z face as the +Z is occupied by the launch vehicle adapter in a position aligned with the CoM of the spacecraft in order to minimize the torque induced by firing the engines, and thus the need for correction burns.

The rest of the 12 other monopropellant 4 N thrusters are placed in the +X/-X and +Y/-Y directions to be able to fully control the attitude of the spacecraft along each axis, each direction and with an almost zero net force. Their location maximizes the lever arm while reducing exhaust impingement on other spacecraft components.

The three main propellant tanks are located at the very center of the structure, oriented along the Z axis and placed side by side in the Y direction. The single oxidizer tank is in the middle, flanked by the two fuel tanks. This configuration allows for low CoM excursions independently of the level of propellant in the tanks, and is close to the center of the spacecraft to reduce its inertia moments.

The auxiliary fuel tank is located besides the battery pack, on the -Z face on its -Y edge.

The pressurizing helium tank is located on the -Z face close to its +Y edge to balance out the mass of the battery and the auxiliary fuel tank.

The whole propulsion system is nearly perfectly symmetrical with respect to the Y-Z plane.

Telecommunications subsystem

The main aspects of this mission under the TTMTTC viewpoint, were the quantity of data to be sent to Earth and the distances reached by the spacecraft. Another peculiar aspect of the design not to be underestimated was the fact that, going inwards in the solar system, the position of the Earth is not fixed in a particular direction: the planet could actually be located in every direction with respect to the spacecraft. Also, it is needed to account for the constraints added by thermal management, mainly connected to the need to always orient the spacecraft in a way to have the shade in the Sun direction.

Hence, the design choices were driven towards a configuration capable of uplink and downlink with Earth without the necessity to orient neither the spacecraft body nor the antennas in a particular direction.

The two identical lightweight, High-gain, Waveguide-Based Phased Array Antennas (PAAs) and two Medium-Gain Fanbeam Antennas (MGA), are conveniently mounted on opposite edges of the spacecraft, in particular the first couple comprehending one PAA and one MGA, is mounted on the front side of the shade corresponding to -X and -Y axis, instead the other one corresponds to +X and +Y axis. The four hemispherical Low-Gain Antennas (LGA) provide coverage in all directions, without the necessity of rotating the spacecraft. Three are mounted on the sunshade, one on the face looking in the -Y direction, the other two on the edges of the sunshade, looking in the directions +Z and -Z; the fourth one is located in the +Y face, looking in the +Y direction.

This design grants not only pointing capabilities by rotating around the spacecraft-Sun line, but also a balanced mass distribution.

The two solid-state power amplifiers are located near each phased array - fanbeam antennas couple to minimize losses.

ADCS subsystem

Four Sun sensors are mounted in the four corners of the sunshield, on the inside face, with the heads of the sensor poking through the shield and with direct line of sight to the Sun. The curvature of the shield allows for differential measures. This is the only body-fixed location available for these sensors, as the only other part of the spacecraft that receives sunlight in the inner cruise phase are the solar arrays, but they can rotate.

Two further Sun sensors are located on the center and +X,-Z corner of the +Y face of the spacecraft, to allow for Sun visibility during the outer cruise.

Two Star trackers are positioned side by side, symmetric with respect to the center line, on the +Y edge of the -Z face, pointed towards the -Z direction. This location was chosen as the Sun will never shine directly in the sensing elements of the star trackers during nominal operations, which may lead to unrecoverable damage.

The inertial measurement unit (IMU), its four gyroscopes and four accelerometers are located under the -X face, close to the spacecraft's CoM to aid precision.

The four reaction wheels are placed in a pyramid configuration. They are located on the -Y face, inside the sunshield, in two pairs that flank the fuel tank: this location was chosen for symmetry reasons with respect to the Y-Z plane and at an X location coincident with the CoM. An added benefit is that not all the torque is applied at the same point on the structure.

Scientific Instruments

The magnetometer MAG needs to be protected by the sunshade but also needs to be far from the possible electromagnetic fields generated close to the spacecraft to operate correctly. Therefore, the only possible direction respecting those requirements is +Y, at the end of a 3.6 m boom (see figure 7.4).

A suite of five "Nadir" pointing instruments (MDIS, MASCS, XRS, MLA, GRS) all require pointing in the direction of Mercury's surface to operate, hence they were all located on the same face and pointed in the same direction that allows the spacecraft to orient itself in a position that would be suitable for all of them at the same time. The location chosen is on the +Z face, to offset the weight of the LVA, battery and tanks on the opposite face. They are located inside the launch vehicle adapter, which itself is aligned with the CoM, to aid symmetric mass distribution, low inertia and a more efficient use of the space (see figure 7.5). The NS doesn't have FOV limitations, and as such is mounted on the -X,-Z corner of the +Y face due to proximity to the data processing unit (DPU).

The EPPS instrument is mounted on the side of the spacecraft, near the top deck (-Z face), and close to the edge of the shade from the sunshield: this allows the instrument to measure ions from Mercury's surface, its magnetosphere, and from the solar wind based on spacecraft orientation.

The FIPS allows for near hemispherical coverage, so positioning is less critical for this instrument. The location chosen was the -X face.

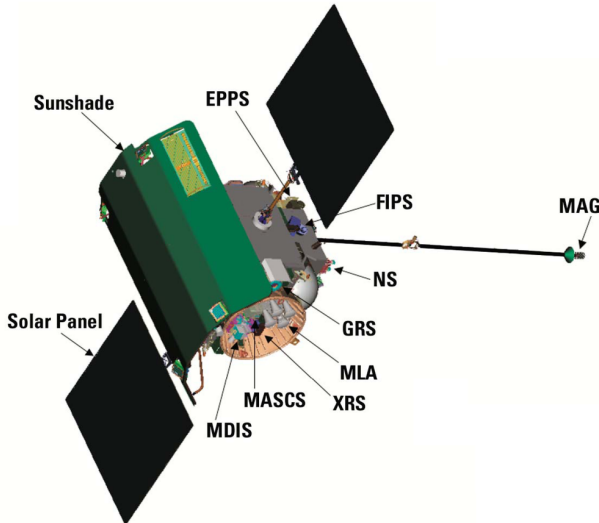


Figure 7.4: Instrument location

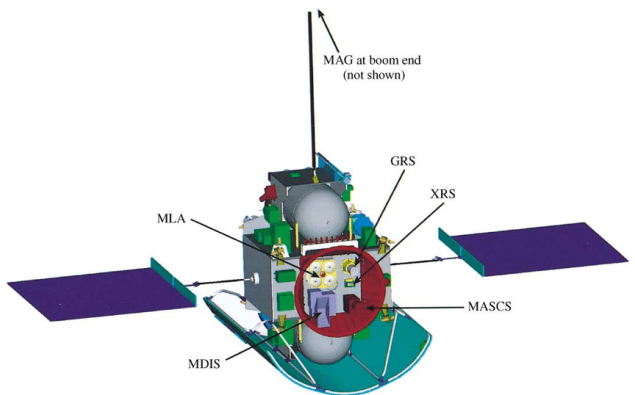


Figure 7.5: Focus on instruments on the $+Z$ face

7.2 On-Board Data Handling

The On Board Data Handling subsystem can be split in different segments: the flight computer architecture, the GNC flight software, and the on-board file storage system; each of them will be analyzed in the following section. The subsystem design has been strongly affected by the mission profile that involves both deep space and near-Sun environment: this imposes constraints including the limited on-board storage, low bandwidth, long light-time delays and intermittent connectivity with Earth [60].

7.2.1 Architecture

Flight computer architecture

MESSENGER is equipped with two sets of flight computers, each of them containing a main processor (MP) operating at 25 MHz and one fault protection processor (FPP) operating at 10 MHz , both of them are *RAD6000* processors with 8 MB of RAM, multiple times space-flight proven. Each couple of MP and FPP, together with other elements, is packaged in an integrated electronics module (IEM) able to provide command and telecommunication functions.

The complete flight software runs in only one active MP performing all nominal operations while both the FPPs monitor the spacecraft safety, the second MP is instead kept unpowered and serves as a backup unit. The following diagram shows the communication links between the flight computers and the GNC hardware components. The databus *MIL-STD-1553* is a military standard federated databus originally developed for avionic systems but widely used also in spacecrafts.

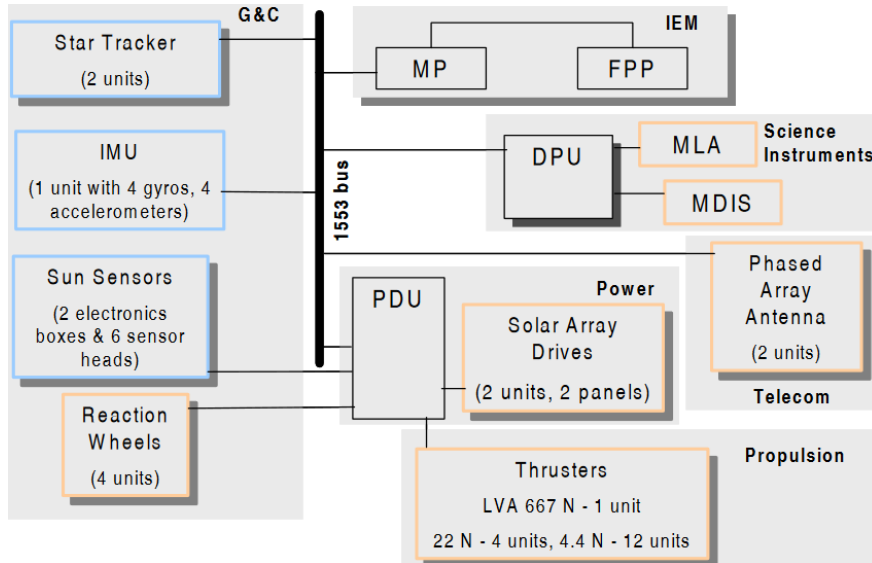


Figure 7.6: On board computer system diagram

The active MP interfaces with the star trackers, the IMU, a redundant Power Distribution Unit (PDU), two Data Processing Units (DPUs) and the two FPPs directly with the 1553 data bus. The PDU interfaces with the Sun sensors, reaction wheels and the propulsion system. The DPU interfaces with all science instruments processor. Both FPPs can access the Sun sensor data and using the GNC software provide an independent Sun direction computation. The Main processor communicates also via peripheral component interconnected (PCI) to a solid state recorded SSR with 8 Gb of RAM [61] [60].

Flight software architecture

MESSENGER on-board software is written in *C* language and is operated under the *VxWorks 5.3.1* real time operating system. The GNC software is composed by six main functional blocks: attitude determination, attitude control, guidance, momentum management, propulsion operations and solar panel control. The GNC Main Processor software functions are split into two main tasks that run at 1 Hz or 50 Hz. Functions necessary for immediate attitude and trajectory control run at 50 Hz and are streamlined to run as efficiently as possible. Attitude determination, solar panel control and all other functions (e.g. phased array antenna steering and MDIS and MLA interfaces) are contained in the 1 Hz tasks [61] [65].

File storage system

MESSENGER uses an on-board file system for data collection based on an 8 Gb Solid State Recorder (SSR). The choice of this sort of system has been driven from two main factors [60]:

- Severely limited downlink capability, because of the combination of available downlink rates, the amount of downlink time and the long round-trip light time. This aspect enforces a constraint on the information stored on-board which needs to be prioritized by importance: in this way it is possible to avoid transmitting in case the bandwidth is not available. A file based system provides simplicity in terms of storing and managing data in terms of priority, making possible to delete the less important data and free space on the SSR;
- Most of science data stored on the SSR are images which come from the Mercury Dual Imaging System (MDIS), compressed and downlinked as individual files by the flight software; this kind of system allows to define variable length images and to compress them using several algorithm options before storing back to the SSR.

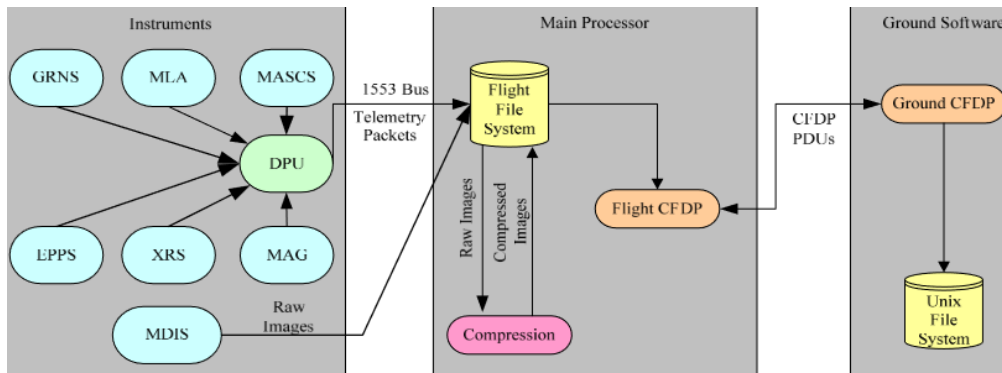


Figure 7.7: Scientific data storage and transfer structure [65]

The flight software has the capability to convert all the telemetry packets, which consist into data concerning the spacecraft activity and science operations, into files [60]. The same goes also for the images from the MDIS instrument, that are stored via a Direct Memory Access (DMA); at a certain point, the software compresses the images through Integer Wavelet Transform (IWT), performs jailbarring of the data and then subframing. IWT is similar to the JPEG compression, allowing for different levels of compression; jailbarring compression operates by removing columns of data and reducing the image; subframing enables to select specific parts of the image for the compression procedure.

The MP can list all the contents in a directory; once a file is completed and ready for downlinking, it is deposited in one of ten directories, each one ranked by priority as it is displayed in Fig 7.8:

- /DNL Prioritized Sub-directories
 - /P0 - Critical OpNavs
 - /P1 - Hskpg Snapshot & Promoted Files
 - /P2 - High Priority Operational Files
 - /P3 - High Priority Science, Health & Safety Files
 - /P4 - Orbit Maintenance/Reconstruction OpNavs
 - /P5 - Prime Science Files (Medium Priority Science)
 - /P6 - Bonus Science Files (Low Priority Science)
 - /P7 - Instrument Burst & Contingency Files
 - /P8 - Autonomy Spawed Engineering Files
 - /P9 - Engineering Contingency Files
- Next Track
- Some Future Track
- Data Recovery Unlikely

Figure 7.8: Directory structure

The files can either be downlinked manually or automatically thanks to the SSR's playback capability: it consists in periodically scanning from P0 to P9, determining if a file exists in any of the directories. After that, a playback list is created, with all the files to downlink in it. Priority ranking and scanning's frequency can change depending on the mission operations, and the presence of a top priority level file could also interrupt the process to ensure that it is downlinked as soon as possible, if necessary.

7.2.2 Reverse Sizing

The first step to size the OBDH system is to list all application functions allocated to the computer. This is done in table (7.1) were the first part contains the data directly obtained from literature [61], while the second one reports the ones deduced from the analysis of the mission architecture.

Device	Measurement or command	Acquisition frequency
IMU	Gyro integrated angular rate	1 Hz and 50 Hz
	Accelerometer integrated linear velocity	50 Hz
	Diagnostic data	1 Hz
Star tracker	Quaternion and rate	1 Hz
	Rate only	50 Hz
	Diagnostic data	1 Hz
Sun sensor	Head ID and Sun aspect angles	1 Hz
SADA	Reference and potentiometer voltages	1 Hz
	Step commands	1 Hz
Reaction wheel	Tachometer time pulse information	50 Hz
	Wheel torque commands	50 Hz
Thrusters	On/off commands	50 Hz
Latch valves	Open/close commands	1 Hz
Heaters	On/off commands	1 Hz
Phased-array antennas	Steering commands	1 Hz

Device	Measurement or command	Acquisition frequency
Instruments	Pointing and data logging	1 Hz
Attitude control	Complete attitude control software	50 Hz
Attitude determination	Complete attitude determination software	1 Hz
Orbit propagation	Orbit propagation software	1 Hz
Complex ephemerides	Planets and stars ephemerides	1 Hz
Engine control	LVA control software	50 Hz
Pressure sensors	Read pressure transducer data	1 Hz
Uplink	Receive and decode uplink data	1 Hz
Downlink	Encode and transmit downlink data	1 Hz
Operating system	Low-level on board software	50 Hz

Table 7.1: Acquisition frequencies of the functions allocated to the MP

Notice that in general only a subset of the previous functions will be executed simultaneously for each flight mode. Nevertheless this analysis considers a worst-case scenario thus the sizing condition accounts for all of the aforementioned functions executed at the same time.

Knowing the acquisition frequency for a given function, the throughput is computed *by-similarity*:

$$KIPS = \frac{KIPS_{typ} \cdot f}{f_{typ}} \quad (7.1)$$

The number of code and data words per function, instead, doesn't need to be adjusted according to the frequency. The total throughput, code and data are obtained by summing the values required by each function.

Component	Number	Code (words)	Data (words)	Throughput (KIPS)
IMU	1	800	500	90
Star tracker	2	2000	15000	200
Sun sensor	2	500	100	1
SADA	2 x 2 <i>funct</i>	2000	1000	1
Reaction wheel	4 x 2 <i>funct</i>	1000	300	125
Thrusters	16	600	400	30
Latch valves	9	800	1500	30
Heaters	17	800	1500	30
Phased array antennas	2	2000	1000	1
Instruments	7	2000	6500	1
Attitude control	1	24000	4200	300
Attitude determination	2	15000	3500	15
Orbit propagation	1	13000	4000	20
Complex ephemerides	1	3500	2500	8
Engine control	1	1200	1500	50
Pressure sensors	5	800	1500	30
Uplink	1	1000	4000	0.7
Downlink	1	1000	2500	0.3
Software	1	15400	7300	180
Total		163300	170500	3504
Total margined		816500	852500	17520

Table 7.2: Code words, data words and KIPS per component

It is important to note that the values in table (7.2) are typical values, that in reality could vary significantly, therefore a margin of 400 % has been included in the calculations.

Transforming data and code words in Kb (considering 32 bit words) it is then possible to calculate the ROM and RAM size:

$$ROM = CODE[Kb] \quad RAM = CODE[Kb] + DATA[Kb] \quad (7.2)$$

The results shown in table (7.3) considers the worst case operative condition that occurs in the orbital phase where all the subsystems are considered simultaneously active except for the main engine control. The ROM is nevertheless sized to account for the complete code while the RAM and throughput are sized according to the aforementioned condition.

	ROM [Mb]	RAM [Mb]	Throughput [MIPS]
Reverse sizing	3.24	6.62	17.27
Real processor	4	8	20

Table 7.3: Memory and performance sizing results [60] [62]

The *RAD6000* processor chosen for the mission satisfies both memory and CPU needs.

Bibliography

- [1] Deborah L. Domingue Alice F. Berman. *Orbital Operations Planning and Scheduling for the MESSENGER Mission*. Tech. rep.
- [2] Eric J. Finnegan Peter D. Bedini. *MESSENGER: An Extreme Systems Engineering Challenge*. Tech. rep. 2010.
- [3] Sean C. Solomon. *MESSENGER Mission Overview*. Tech. rep. 2007.
- [4] James V. McAdams. *MESSENGER Mission Design and Navigation*. Tech. rep. 2007.
- [5] Brian R. Page. *MESSENGER NAVIGATION OPERATIONS DURING THE MERCURY ORBITAL MISSION PHASE*. Tech. rep.
- [6] Deborah L. Domingue Alice F. Berman. *Testing and validation of orbital operations plans for the MESSENGER mission*. Tech. rep.
- [7] Robin M. Vaughan. *Return to Mercury: The MESSENGER Spacecraft and Mission*. Tech. rep. 2006.
- [8] Andrew G. Santo. *The MESSENGER mission to Mercury: spacecraft and mission design*. Tech. rep. 2000.
- [9] Sean C. Solomon. *The MESSENGER mission to Mercury: scientific objectives and implementation*. Tech. rep. 2000.
- [10] Katie Dommer Sam Wiley. *MESSENGER Propulsion System Flight Performance*. Tech. rep. 2000.
- [11] John Hopkins University Advanced Physics Laboratory. *MESSENGER*. <https://messenger.jhuapl.edu/>.
- [12] John Hopkins University Advanced Physics Laboratory. *Messenger Orbital Elements*. <https://messenger.jhuapl.edu/About/mission-design/details-propulsion-activity/MOE.xls>.
- [13] NASA. *Messenger mission*. <https://solarsystem.nasa.gov/missions/messenger/in-depth/>.
- [14] JHUAPL NASA. *MESSENGER Mercury Orbit Insertion Press Kit*. Tech. rep. 2011.
- [15] Larry Mosher Sam Wiley Katie Dommer. *Design and Development of the Messenger Propulsion System*. Tech. rep. 2003.
- [16] Carl S. Engelbrecht Sam Wiley Katie Dommer. *MESSENGER Propulsion System Flight Performance*. Tech. rep. 2006.
- [17] Michael D. Trela Marc N. Wilson Carl S. Engelbrecht. *Flight Performance of the MESSENGER Propulsion System from Launch to Orbit Insertion*. Tech. rep. 2012.
- [18] Johns Hopkins Applied Physics University. *Messenger Mission Design, Launch and Cruise*. Tech. rep.
- [19] Carl S. Engelbrecht Sam Wiley Katie Dommer. *MESSENGER Propulsion System Flight Performance*. Tech. rep. 2006.
- [20] L.Paal. *34-m and 70-m Telemetry reception*. Tech. rep. 2006.
- [21] Michael D. Trela Marc N. Wilson Carl S. Engelbrecht. *Flight Performance of the MESSENGER Propulsion System from Launch to Orbit Insertion*. Tech. rep. 2012.
- [22] Karl B. Fielhauer Dipak K. Srinivasan Mark E. Perry. *The Radio Frequency Subsystem and Radio Science on the Messenger Mission*. Tech. rep. 2007.
- [23] Ralph L. McNutt Andrew g. Santo Robert E. Gold. *The MESSENGER mission to Mercury: spacecraft and mission design*. Tech. rep. 2001.
- [24] S. Dolinar K. Andrews V. Stanton. *Turbo-Decoder Implementation for the Deep Space Network*. Tech. rep. 2002.
- [25] James McAdams Carl J Ercol David F. Persons. *Return to Mercury: the MESSENGER spacecraft and mission*. Tech. rep. 2006.
- [26] Sheng Cheng Robert E. Wallis. *Phased-Array Antenna System for the MESSENGER Deep Space Mission*. Tech. rep. 2006.
- [27] Ralph L. McNutt Sean C. Solomon. *MESSENGER Mission Overview*. Tech. rep. 2007.
- [28] MESSENGER: An Extreme System Engineering Challenge. *Peter D. Bedini, Eric J. Finnegan*. Tech. rep. 2010.

- [29] Johns Hopkins Applied Physics University. *MESSENGER Mission: First Electronically Steered Antenna for Deep Space Communications*. Tech. rep.
- [30] Robert E. Wallis Perry M. Malouf. *The Medium-gain Antenna of the MESSENGER Spacecraft*. <https://www.microwavejournal.com/articles/606-the-medium-gain-antenna-of-the-messenger-spacecraft>.
- [31] Dong K. Shin. *Frequency and Channel Assignments*. Tech. rep. Jet Propulsion Laboratory, 2020.
- [32] NASA. *2022 SOA Communications Chapter*. Tech. rep. 2022.
- [33] Monty Andro FuqinXiong. *The Effect of Doppler Frequency Shift, Frequency Offset of the Local Oscillators, and Phase Noise on the Performance of Coherent OFDM Receivers*. Tech. rep. 2001.
- [34] Daniel J. O'Shaughnessy Sarah H. Flanigan Robin M. Vaughan. *Guidance and Control of the MESSENGER spacecraft in the Mercury Orbital Environment*. Tech. rep. 2012.
- [35] Robert E. Gold et al. *The MESSENGER mission to Mercury: scientific payload*. Tech. rep. 2001.
- [36] M. Lavagna. *Space System Engineering and Operations*. 2022-2023.
- [37] Robert E. Gold et al. *The MESSENGER mission to Mercury: spacecraft and mission design*. Tech. rep. 2001.
- [38] Carl S. Engelbrecht Marc N. Wilson. *Flight performance of the MESSENGER propulsion system from launch to orbit insertion*. Tech. rep. 2012.
- [39] Northrop Grumman Corporation. *SIRU - Scalable Inertial Reference Unit for Space*. Tech. rep.
- [40] Carl J. Ercol Edward D. Shaefer Vincent L. Bailey. “Spacecraft Packaging”. In: (2008).
- [41] Marshall Space Flight Center M. M. Finckenor. “Multilayer Insulation Material Guidelines”. In: (1999).
- [42] George Dakermanji James C. Leary Richard E. Conde. “The MESSENGER spacecraft”. In: (2006).
- [43] Carl J. Ercol G. Allan Holtzman Shawn M. Begley. “Return to Mercury: An overview of the MESSENGER Spacecraft Thermal Environmental Prediction and Analysis Process”. In: (2015).
- [44] Carl J. Ercol G. Allan Holtzman Shawn M. Begley. “Return to Mercury: An overview of the MESSENGER spacecraft thermal control system design and update on orbital flight performance”. In: (2012).
- [45] H. Evans J. Sorensen. *Mercury environmental specification (part III)*. Tech. rep. 2004.
- [46] 3M Nextel. *3M Nextel ceramic fibers and textiles technical reference guide*.
- [47] Kenneth E. Hibbard Kimberly J. Ord. “MESSENGER Power and Thermal Systems Operations”. In: (2010).
- [48] Carl J. Ercol. “The MESSENGER spacecraft Power and Thermal Performance through mercury Flyby 3”. In: (2010).
- [49] Carl J. Ercol. “Return to Mercury: An Overview of the MESSENGER Spacecraft Thermal Control System Design and Up-to-Date Flight Performance”. In: (2006).
- [50] James R. Wertz Wiley J. Larson. “Space Mission Analysis and Design”. In: () .
- [51] John Stark Peter Fortescue Graham Swinerd. “Spacecraft Systems Engineering 4th Edition”. In: () .
- [52] Carl J. Ercol. “The MESSENGER Spacecraft Power Subsystem Thermal Design and Early Mission Performance”. In: () .
- [53] David F. Persons Paul D. Wienhold. *The development of high-temperature composite solar array substrate panels for the messenger spacecraft*. Tech. rep.
- [54] J. Jenkins G. Dakermanji C. Person. *The MESSENGER spacecraft power system design and early mission performance*. Tech. rep.
- [55] Kimberly J. Ord and Kenneth E. Hibbard. *MESSENGER Power and Thermal Systems Operations*. Tech. rep.
- [56] Richard F. Conde James C. Leary and George Dakermanji. *The MESSENGER Spacecraft*. Tech. rep.
- [57] Binh Le C. Jack Ercol George Dakermanji. *The MESSENGER spacecraft power subsystem thermal design and early mission performance*. Tech. rep.
- [58] European Space Agency. *Margin philosophy for science assessment studies*. Tech. rep. 2012.
- [59] United Launch Alliance. *Delta II Payload Planners Guide*. Tech. rep. 2006.
- [60] Christopher J. Krupiarz et al. *File-based data processing on MESSENGER*. Tech. rep. 2005.

- [61] Robin M. Vaughan et al. *THE MESSENGER SPACECRAFT GUIDANCE AND CONTROL SYSTEM*. Tech. rep. 2005.
- [62] BAE SYSTEMS. *RAD6000™ Space Computers*. Tech. rep. 2006.
- [63] Robin M. Vaughan et al. *Return to Mercury: The MESSENGER Spacecraft and Mission*. Tech. rep. 2006.
- [64] Robert E. Gold et al. *The MESSENGER mission to Mercury: scientific payload*. Tech. rep. 2001.
- [65] David A. Artis et al. *MESSENGER: Flight Software Design for a Deep Space Mission*. Tech. rep. 2007.